Table of Contents

1. Material and Methods

Expression and Purification of KRAS. Human KRAS protein (residues 1-185) bearing a single C118S mutation was expressed as the post-translationally unprocessed form from *Escherichia coli* BL21 (DE3) cells using the pET-28 vector that encodes the protein with the N-terminal hexa-histidine tag followed by a thrombin cleavage site. The cells were grown at 37°C in M9 media containing 4 g/L of glucose and 1 g/L NH_4Cl to an optical density (OD_{600}) of 0.3-0.4, at which the media was supplemented with 60 mg/mL 2-ketobutyric acid-4-^{13}C and 100 mg/mL of 2-keto-3-(methyl-^{13}C)-butyric acid to ^{13}C label the methyl groups of the Ile-Cδ1, and the Leu-Cδ and Val-Cγ, respectively. Expression was induced with 0.25 mM isopropyl β-D-1-thiogalactopyranoside (IPTG) at 15°C and an OD_{600} of 0.6 for 16 h. For selective labeling of Lys ^{15}N-amides, the cells were grown 37°C in M9 media containing 4 g/L glucose, 1 g/L NH_4Cl and 100 mg/L of each of the 19 unlabeled amino acids to an optical density (OD_{600}) of 0.6-0.8, at which the media was supplemented with 100 mg/L ^{15}N-Lys and 500 mg/L of each of the unlabeled amino acids. After 15 min, expression was induced with 1 mM IPTG, and the culture was incubated at 37°C for 2 h to minimize isotope scrambling. The protein was initially purified using the Ni^{2+} affinity column, followed by thrombin digestion overnight at room temperature to remove the histidine tag, and final purification using size exclusion chromatography (Superdex 75; GE Healthcare) in a pH 7.4 buffer consisting of 50 mM HEPES, 100 mM NaCl, and 5 mM $MgCl_2$. Fully processed KRAS (FP-KRAS), which contains the farnesylated and methylated Cys185 at the C-terminus, was obtained from the baculovirus-insect cell (Hi5) expression system, as described previously[1]. To carry out NMR experiments, FP-KRAS was isotopically labeled with ^{13}C-[Ile, Leu, Val, Thr] by supplementing 150 mg/L ^{13}C-Ile, 100 mg/L ^{13}C-Leu, 50 mg/L ^{13}C-Val and 75 mg/L ^{13}C-Thr in an insect cell media deficient of these amino-acids 16 h after the baculovirus infection. Two single-cysteine mutants (S39C and K169C) and three charge-reversal mutants (R135E, E168R, an R135E/E168R) of KRAS were made by the standard mutagenesis protocol.

Preparation of Nanodisc-tethered KRAS. The lipid bilayer nanodiscs encircled by two copies of membrane scaffold protein 1D1 (MSP1D1) were prepared at a 40:1 molar ratio of MSP1D1:lipid according to the published protocol[2]. This type of nanodisc has a small size with a leaflet diameter of ~ 10 nm and a molecular weight of ~ 120 kDa[3]. All lipids were purchased from Avanti Polar Lipids, Inc., including 1,2-dioleoyl-sn-glycero-3-phosphocholine (DOPC), 1,2-dioleoyl-sn-glycero-3-phospho-L-serine (DOPS), 1,2-dioleoyl-sn-glycero-3-phosphoethanolamine-N-[4-(p-maleimidomethyl)cyclohexane-carboxamide] (PE-MCC), and 1,2-distearoyl-snglycero-3-phosphoethanolamine-N-diethylenetriaminepentaacetic acid (PE-DTPA). They were mixed at a molar ratio of 72.5:20:5:2.5 to produce 20% phosphatidylserine (PS)-

containing nanodiscs. MSP1D1 was produced from *Escherichia coli* BL21 (DE3) cells with the pGBHPS-MSP vector in 2× yeast extract tryptone media using a LEX bioreactor system. Expression was induced at 37 °C with 1 mM IPTG at an OD_{600} of 2.5 for 1 h, followed by further incubation at 28 °C for 2.5 h. The protein was purified using the Ni^{2+} affinity column, followed by His_6-GB1 tag cleavage with HRV3C protease and subsequent size exclusion chromatography (Superdex 75; GE Healthcare) in a pH 7.4 buffer consisting of 50 mM HEPES, 100 mM NaCl, and 5 mM $MgCl_2$. Nanodisc maleimide-conjugated KRAS (MC-KRAS) was prepared by conjugation of the C-terminal cysteine (Cys185) of a KRAS mutant (C118S) to PE-MCC for 16 h at room temperature. To separate membrane-associated MC-KRAS from free KRAS in solution, the mixture was subjected to size exclusion chromatography (Superdex 200; GE Healthcare) in a final buffer (pH 7.4) containing 50 mM HEPES, 100 mM NaCl, and 5 mM $MgCl_2$. For nucleotide exchange, the GDP-loaded KRAS were incubated overnight at 4°C with a 10-fold molar excess of GTPγS and 10 mM EDTA.

Preparation of the NS1 Monobody. According to the previous protocol[4], the NS1 monobody was expressed as a fusion protein with the N-terminal hexa-histidine tag followed by a biotin-acceptor tag and a TEV cleavage site from *Escherichia coli* BL21 (DE3) cells with the vector pHBT. The protein was purified using the Ni^{2+} affinity column, followed by TEV cleavage to remove the histidine tag and final purification with size exclusion chromatography (Superdex 75; GE Healthcare).

NMR Experiments. NMR measurements were carried out at 288 K on Bruker AVANCE III HD 700- and 800-MHz spectrometers equipped with a 5-mm TCI CryoProbe. All NMR samples were dissolved in a pH 7.4 buffer consisting of 50 mM HEPES, 100 mM NaCl, 5 mM $MgCl_2$, and 10% (vol/vol) D_2O. For one-dimensional (1D) NMR titration experiments, 40 μM MC-KRAS were titrated with increasing molar equivalents (1, 2, 3, 4, 5, 6, 8, and 10) of fully processed KRAS (FP-KRAS). For PRE experiments, two-dimensional (2D) ^{1}H-^{13}C TROSY[5] or ^{1}H-^{15}N HSQC spectra of 80 μM MC-KRAS were collected in the presence and absence of the same concentration of FP-KRAS. Spin labels, such as TEMPO (Toronto Research Chemicals), 5% Gd^{3+}- or Cu^{2+}-chelated PE-DTPA, and 2 mM Gd-DTPA-BMA, were incorporated into the SH group of one of three cysteines (Cys39, Cys118, and Cys169) of FP-KRAS, nanodiscs, and bulk solvent, respectively. A concentrated stock of TEMPO in acetonitrile was added at a 5:1 molar ratio of TEMPO to KRAS, and the mixture was incubated at 4°C for 16 h and dialyzed at 4°C for 8 h into NMR buffer to remove the residual TEMPO reagent. For diamagnetic control experiments, 0.8 mM ascorbic acid was added as a reducing agent into samples containing 80 μM TEMPO spin label, and the mixture was incubated at 15°C for at least 2 h to ensure complete reduction of the TEMPO spin. Lu^{3+}-chelated PE-DTPA

was used as a diamagnetic lipid to replace paramagnetic Gd^{3+}- or Cu^{2+}-chelated PE-DTPA. The peaks were assigned based on assignments deposited in the Biological Magnetic Resonance Data Bank (BMRB) (entry number: 17610, 17785, 25115, 27472, and 30401), and ambiguous assignments were resolved by selective isotope-labeling of each of Ile, Leu, Val, and Thr of FP-KRAS, as well as 2D TOCSY- and NOESY-type experiments.

PRE Analysis. NMR data were processed and analyzed with the NMRPipe[6] and NMRView[7] softwares. The intensities of the cross-peaks were measured with Lorentzian line shape fitting of the program nlinLS in the NMRPipe software package[6]. The transverse relaxation rate in the diamagnetic state, R_2, was estimated from the half-height line width of each peak by employing the method reported by Wagner and co-workers[8]. Overlapped cross-peaks on the spectra were excluded in the analysis. In TEMPO-PRE experiments, the peak intensities were referenced to the ^{1}H peak intensity of 4,4-dimethyl-4-silapentane-1-sulfonic acid (DSS) that is dissolved in the same sample although a pair of the two spectra was obtained in the same sample concentrations and NMR acquisition parameters. PRE effects on the individual probes of KRAS were assessed by the intensity ratios of the paramagnetic to diamagnetic peaks (I_{para}/I_{dia}). These values were converted into the ^{1}H transverse PRE rate (^{1}H-Γ_2) with the equation 1 as follows:

$$\frac{I_{para}}{I_{dia}} = \frac{R_2 \times \exp(-\Gamma_2 \times t)}{R_2 + \Gamma_2} \qquad \text{(equation 1)}$$

where t is the total INEPT evolution time in the NMR pulse sequence. The PRE effect on ^{1}H longitudinal relaxation rate (^{1}H-R_1) is typically negligible because it is much smaller than ^{1}H-Γ_2. The paramagnetic relaxations of ^{15}N and ^{13}C nuclei were ignored in the analysis because they have much lower gyromagnetic ratios than ^{1}H nucleus. The ^{1}H-Γ_2 values were converted into distances (r) between observed protons and the paramagnetic spin label by using the equation 2 as follows:

$$r = \sqrt[6]{\frac{F_{dimer}}{\Gamma_2}\frac{\gamma_H^2 g_e^2 \beta^2 \mu_0^2 (S+1)S}{240\pi^2}\left(4\tau_c + \frac{3\tau_c}{1+\omega_H^2\tau_c^2}\right)} \qquad \text{(equation 2)}$$

where F_{dimer} is the fraction of KRAS dimer, γ_H is the proton nuclear gyromagnetic ratio, g_e is the electronic

g factor, β is the Bohr magneton, μ_0 is the vacuum permeability, S is the spin quantum number for free electrons, ω_H is the proton Larmor frequency, and τ_c is the rotational correlation time of the electron-nucleus vector. τ_c was assumed to be equal to the global correlation time of the complex. Different sets of distances were calculated from a variable F_{dimer} with the equation 2. In the analysis of the Gd^{3+}/Cu^{2+}-PRE data, net $^1H\text{-}\Gamma_2$ values of the KRAS dimer were extracted from a mixture of $^1H\text{-}\Gamma_2$ of the monomeric and dimeric species with the following equation 3, assuming that the monomer-dimer equilibrium is in the fast exchange regime on the Γ_2 relaxation time scale.

$$^1H\text{-}\Gamma_{2,app} \approx F_{mono} \times {}^1H\text{-}\Gamma_{2,mono} + F_{dimer} \times {}^1H\text{-}\Gamma_{2,dimer} \qquad \text{(equation 3)}$$

where $^1H\text{-}\Gamma_{2,app}$ is the population-weighted average of $^1H\text{-}\Gamma_{2,mono}$ and $^1H\text{-}\Gamma_{2,dimer}$, which represent $^1H\text{-}\Gamma_2$ values for the monomeric and dimeric states of MC-KRAS, respectively, and F_{mono} and F_{dimer} represent the relative fractions of the monomeric and dimeric states, respectively.

Building the Structures of KRAS Dimers on the Nanodisc. Unambiguous distance restraints for defining the dimer interface between two KRAS protomers were derived from the TEMPO-PRE data of MC-KRAS that exhibit the I_{para}/I_{dia} values of < 0.8. Variable sets of distance restraints were calculated by changing the F_{dimer} value (0.05, 0.1, 0.2, 0.4, 0.6, and 0.8 and 1.0) in equation 2. In the analysis of the TEMPO-PRE data of FP-KRAS, additional distance restraints for $^{13}C\gamma$-methyl probes were generated with the F_{dimer} value that is calculated from the optimized F_{dimer} (0.1) multiplied by the $^1H\text{-}\Gamma_2$ ratio between the reference probes commonly included in FP- and MC-KRAS. To account for errors in the estimate of $^1H\text{-}\Gamma_2$, distance restraint bounds were set to ± 3 Å from the calculated distance. The r^{-6} dependency of $^1H\text{-}\Gamma_2$ markedly reduces the uncertainty of distances in the PRE analysis. Negative distance restraints for isotopic probes with no large PREs with I_{para}/I_{dia} of > 0.9 were created in such a manner that the lower distance limit is set to be - 3 Å from the distance calculated from the I_{para}/I_{dia} ratio of 0.9. These restraints enforce the absence of close interactions between the related atoms. Distance restraints between the KRAS dimer and lipid headgroups on one leaflet of the nanodisc were derived from the membrane PRE data of MC-KRAS that exhibit both the I_{para}/I_{dia} values of < 0.6 (Gd^{3+}-PRE) or < 0.8 (Cu^{2+}-PRE) in the presence of FP-KRAS and the $\Delta^1H\text{-}\Gamma_{2,di\text{-}mono}/^1H\text{-}\Gamma_{2,mono}$ values of > 0.3 upon addition of FP-KRAS. Distance restraints were set for six lysines (K172 and K175-K179) in the C-terminal HVR in both the GTP- and GDP-bound states, which show relatively high Cu^{2+}-PREs with I_{para}/I_{dia} of < 0.6 regardless of dimerization. Distance restraints were set for probes

V44γ and V45γ in the GDP-bound state, which show relatively high Gd^{3+}-PREs with I_{para}/I_{dia} of < 0.4 in the presence of FP-KRAS. These distance restraints were determined in a semi-quantitative fashion that the lower limit was set to - 10 Å from the distances calculated from the optimized F_{dimer} (0.1). This relatively wide error margin was chosen considering dynamic factors to reduce the apparent PRE effects: (i) highly diffusive paramagnetic lipids on the membrane surface and (ii) mobility of the KRAS dimer on the membrane. For membrane association of the C-termini of two KRAS protomers, an upper limit of 2 Å was set as an ambiguous restraint for Lys184. Distances from PRE-observed heavy atoms (C and N) to both spin-labeled gamma positions of KRAS and lipid headgroup atoms on one leaflet of the nanodisc were set in a symmetric manner for two KRAS protomers. The conformational ensemble of the KRAS dimer on the nanodisc was generated using the standard multi-body docking protocol embedded in the HADDOCK 2.2 software[9]. The starting nanodisc model was generated by incorporating a lipid bilayer containing 80% DOPC and 20% DOPS, computed via CHARMM-GUI[10], into an MSP1D1 nanodisc model[3]. To construct the starting KRAS model, the crystal structures of the closest to the full-length KRAS (residues 1-180, PDB ID: 4DSO for GTPγS-bound state and 4DSU for GDP-bound state) were modified by incorporating residues 181-184, and then they were subjected to energy minimization in the CNS software[11]. The C-terminal residues 172-184 were assigned fully flexible based on the elongation of the C-terminal helix 5 shown in the crystal structures. According to the sampling protocol, 3000 complex structures were generated in the first step of the rigid body docking, 400 structures were selected in the semi-flexible docking, and 200 structures were finally submitted to the water refinement steps. The coordinates of the 20 best HADDOCK structures of KRAS homodimers are deposited in the Protein Data Bank (accession number: 6W4E for the GTPγS-bound state and 6W4F for the GDP-bound state). Violation analysis of PRE-derived distances in the final HADDOCK model was performed using a modified Q-factor[12], a value that represents the agreement between distance observed from PRE experiment (r^{obs}) and HADDOCK model distance (r^{model}), defined as:

$$\text{Q-factor} = \sqrt{\frac{\sum_i \{r^{obs}(i) - r^{model}(i)\}^2}{\sum_i r^{obs}(i)^2}} \qquad \text{(equation 4)}$$

2. Supplemental Results for HADDOCK Models

A set of 200 final structures was generated with variable sets of distance restraints calculated by changing the fraction of observed MC-KRAS sample (F_{dimer}) bound to the paramagnetic FP-KRAS in equation 2 in the Material and Methods section. Goodness-of-fit of distances were assessed by the standard distance restraint potential, E_{noe} (Figure S12). The lowest E_{noe} values were found with a F_{dimer} of 0.1. The optimized F_{dimer} value agrees well with the F_{dimer} values of 0.12 (GTPγS state) and 0.11 (GDP state) calculated based on the concentration and the experimentally derived K_D values for KRAS dimerization.

The PRE-derived distances of KRAS-GTPγS do not agree with the KRAS-GDP structure, or vice versa. Violations of PRE-derived distances in the reference structure of the KRAS dimer in each nucleotide state are evaluated using a Q-factor (Figure S13 and Table S2) as defined in equation 4 in the Material and Methods section.

Inspection of the HADDOCK reference structure of KRAS-GTPγS homodimer revealed that one of the protomers is more intimately associated with the membrane surface. Because our system recognizes FP- and MC-KRAS as distinct entities, the cluster comprises two sub-clusters that are symmetrically related and differ only in which protomer interacts more closely with the membrane. In all of the structures, the two protomers engage with each other in the same mode of binding, although some variability was observed in the details of the protein-membrane interface, which may reflect a 'fuzzy' interaction or the result of a limited number of restraints. In the 200 and 20 lowest HADDOCK-score structures of the GTPγS-bound dimer, the tilt angles of the dimer interface plane, defined by two interfacial α4 and α5 helices, with respect to the membrane surface are 78 ± 5° and 80 ± 4°, respectively, whereas the GTPase domain alone (residues 1-172, lacking the C-terminal flexible region and the membrane) superimpose very well with average backbone RMSDs of 0.68 ± 0.21 Å and 0.61 ± 0.13 Å, respectively, to the mean structures, indicating that the dimer interface itself is well-defined (Figure S14). In the analysis of the GDP-bound KRAS dimer, the 200 and 20 HADDOCK models converged on a more tightly defined cluster, with tilt angles of 83 ± 3° and 84 ± 3°, respectively. The RMSDs for the GTPase domain alone were 0.95 ± 0.35 Å and 0.94 ± 0.26 Å, respectively (Figure S15). Statistics for the 20 best HADDOCK structures are described in Table S1.

In addition, in the 10 best models of the GTPγS-bound dimers, the protomers exhibit an orientation in which α5 is perpendicular to the membrane with a minimum angle of 75 ± 8° between the axis of α5 and the membrane surface, while this orientation is semi-perpendicular in the GDP-bound dimers, with an angle of 51 ± 5°. These membrane orientations are significantly different from those we previously described for KRAS monomers[2b]: those "exposed" and "occluded" states exhibit parallel and semi-parallel orientations of the α5 axis with respect to the membrane, with angles of 3 ± 7° and 36 ± 9°, respectively.

The dimer interface buries 632 ± 55 Å^2 and 770 ± 96 Å^2 of surface area per protomer in 20 KRAS dimer structures in the GTPγS- and GDP-bound states, respectively, and the buried surfaces in these two states overlap but are partly distinct (Figure S16).

3. Supplemental Discussion for Biological Roles of KRAS Dimerization

As many signaling proteins such as small GTPases are lipidated, a number of cell signaling events take place at the membrane surface. The biological membrane provides a platform that promotes protein-protein interactions involved in the regulation of important biological processes. In line with this view, our structural data on KRAS dimerization, in combination with our previous report that KRAS monomers preferentially adopt certain orientations[2b], suggest that these factors dictate how it can interact with downstream effectors such as RAF kinases, leading to their activation. The KRAS-GTP monomer favors an orientation in which the membrane occludes the effector binding site (β-interface), while the α4-α5 dimer interface (α-interface) is exposed[2b]. Comparison between this occluded state and the present KRAS-GTPγS dimer model reveals that the dimerization releases the occlusion of the β-interface, which would facilitate productive binding of KRAS to the RAS binding domain (RBD), and the orientation of our KRAS-GTPγS dimer suggests each KRAS protomer could simultaneously interact with a RBD, which may promote dimerization of the RAF kinase domain[13]. This process could also promote direct association of the RAF Cysteine-Rich Domain (CRD) with membrane phospholipids. The functional relevance of KRAS-GDP dimerization remains unknown, but the structure appears incompatible with the guanine nucleotide exchange factor (GEF) SOS1-mediated GDP/GTP exchange, since the GEF binding site is occluded by the membrane, whereas it is exposed in the major species of the monomeric form (Figure S20).

From a kinetic viewpoint, RAF-RBDs exhibit fast binding rates and high affinity toward the RAS GTPase-domain due to electrostatic steering[14], a mechanism that plays a role in many signaling events. RAF must capture transiently surface-exposed RBD binding sites (β-interfaces) of KRAS, which are promoted by transient formation of KRAS-GTP dimers that preferentially localize in PS-rich lipid domains[15]. The importance of the exposure of the β-interface for recruitment of the RAF-RBD was demonstrated with specific disease-associated KRAS variants that enhance signaling by destabilizing the occluded membrane orientation[2b]. Further, dimerization may modulate the GTPase cycle. Docking of RAS GTPase activating proteins (RasGAPs) is compatible with the structure of the KRAS-GTP dimer (Figure S21B), but not the occluded state of the KRAS monomer on the membrane (Figure S21A), suggesting that dimerization might promote rapid inactivation of KRAS. Indeed, single-molecule fluorescence data showed that RasGAP is recruited to activated RAS signaling complexes[16].

4. Supporting Figures

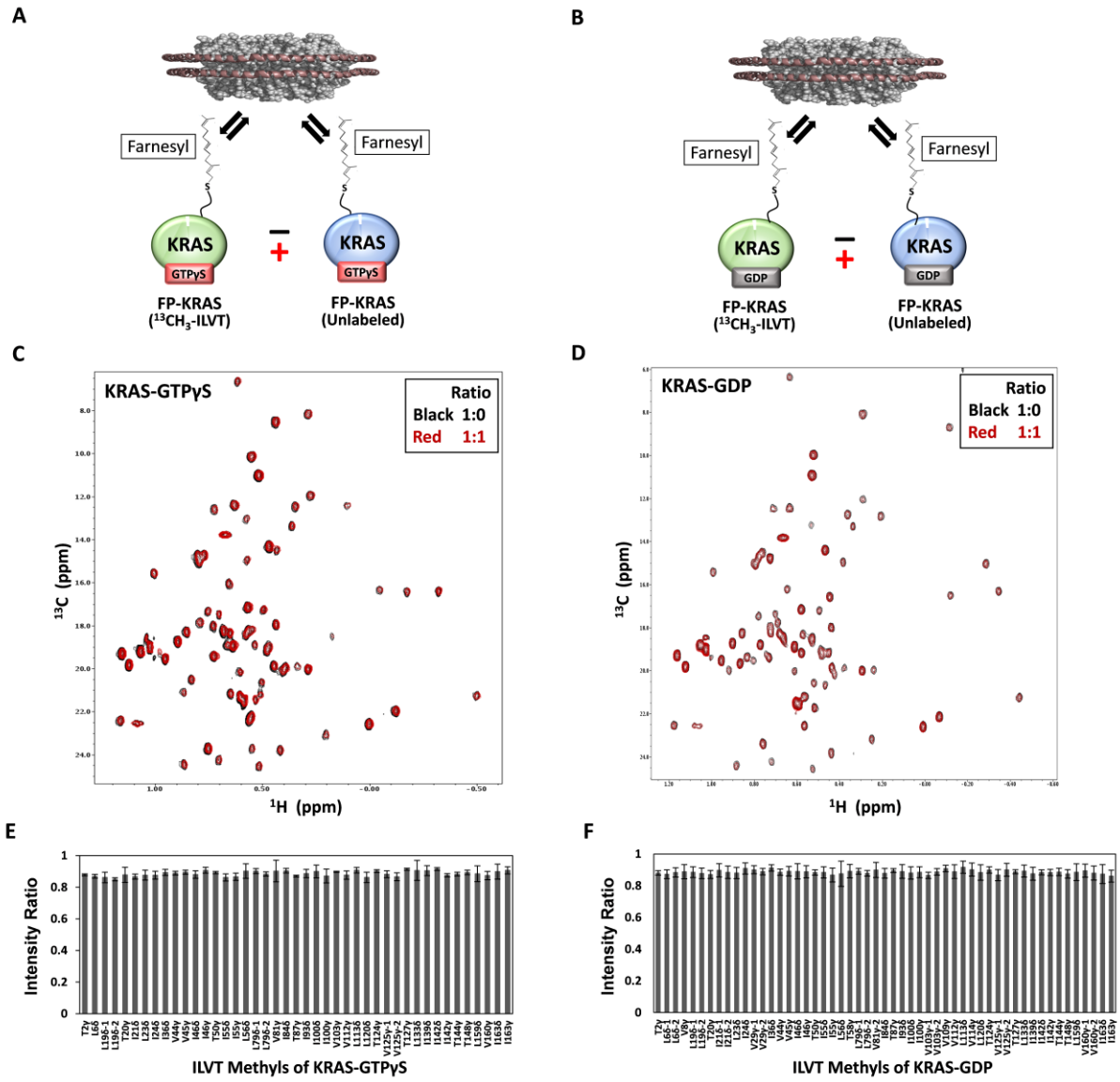

Figure S1. Lack of spectral changes of ^{13}C-labeled FP-KRAS in the presence of nanodiscs upon addition of isotopically unlabeled FP-KRAS. (A, B) Illustration of NMR experimental design with [ILVT-^{13}C methyl]-labeled FP-KRAS, isotopically unlabeled FP-KRAS, and nanodisc. (C, D) Overlay of ^{1}H-^{13}C TROSY spectra of [ILVT-^{13}C methyl]-labeled FP-KRAS with nanodiscs in the presence (red) and absence (black) of an equivalent amount of isotopically unlabeled FP-KRAS. (E, F) Plots of intensity ratios of peaks of ILVT ^{13}C-methyl probes in the spectra in panels (C) FP-KRAS-GTPγS and (D) FP-KRAS-GDP, respectively.

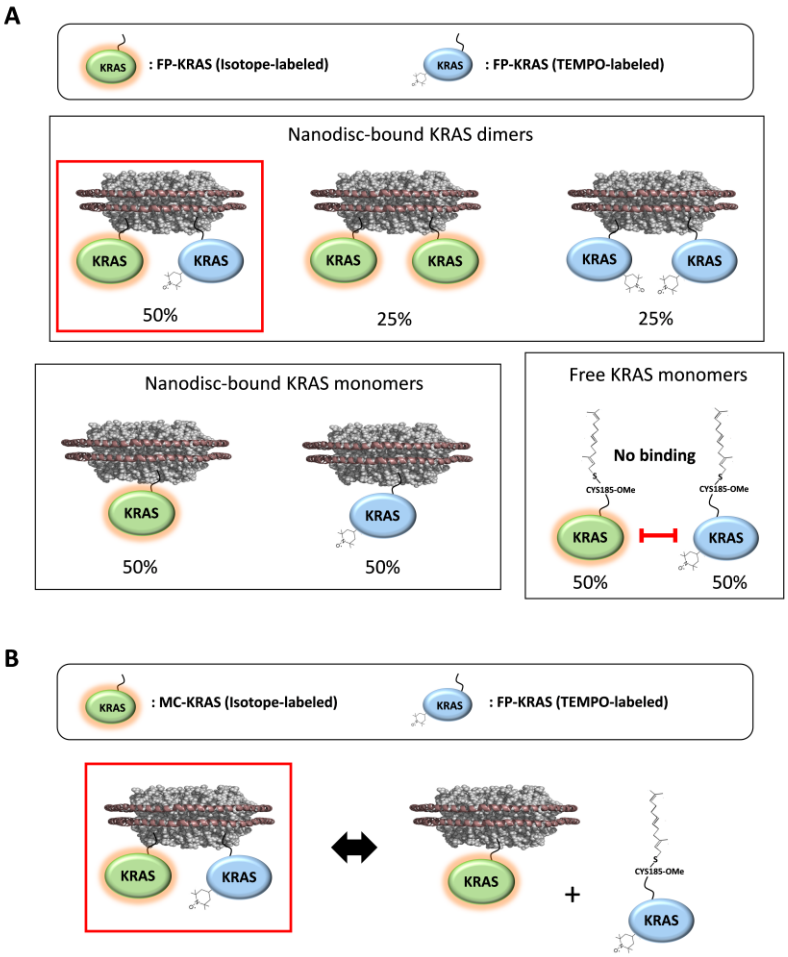

Figure S2. Molecular configurations of KRAS protomers possible in two paramagnetic dimerization systems used in this study. (A) KRAS dimerization system using only fully processed KRAS (FP-KRAS). The system is in equilibrium between three states: free KRAS monomer in solution, as well as nanodisc-bound KRAS monomers and dimers. The nanodisc-bound dimers consist of three combinations of KRAS species: (i) one isotope-labeled and one TEMPO-labeled protomer, (ii) two isotope-labeled protomers, and (iii) two TEMPO-labeled protomers. The probability of occurrence for each combination is indicated. Only dimers with configuration (i) exhibit PRE effects, which would be 'diluted' by the other two states, as well as monomers in solution that do not exhibit PRE. (B) KRAS dimerization system combining maleimide lipid-conjugated KRAS (MC-KRAS) with FP-KRAS. This system is in equilibrium between two states: isotopically labeled MC-KRAS alone and in complex with FP-KRAS on the nanodisc. The NMR signals observed are derived exclusively from nanodisc-associated MC-KRAS, which can be titrated with PRE-tagged FP-KRAS. Red rectangular lines represent dimer configurations that generate intermolecular PRE effects. The enhanced PRE in the MC-KRAS system is the result of promoting 'PRE-competent' dimers consisting of one isotope- and one TEMPO-labeled protomer, enabling more quantitative analyses to calculate the structure of the KRAS dimer.

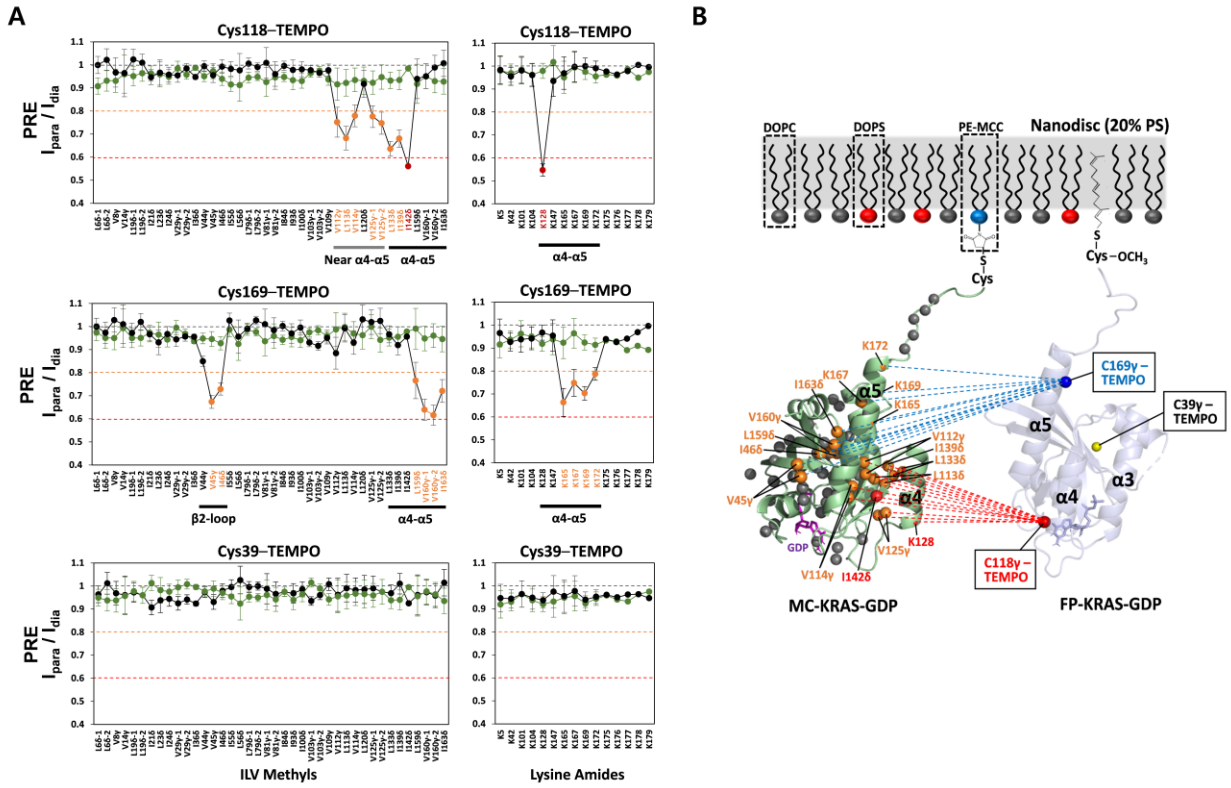

Figure S3. Intermolecular PRE effects between MC-KRAS-GDP and FP-KRAS-GDP. (A) Intensity ratios of peaks in the presence of paramagnetic versus diamagnetic (reduced) spin labels (I_{para}/I_{dia}) for ILV ^{13}C-methyls and Lys ^{15}N-amides of MC-KRAS-GDP in the presence of FP-KRAS-GDP (black lines) and FP-KRAS- GTPγS (green lines) that are tagged with TEMPO at one of Cys118, Cys169, or Cys39. PRE-affected probes are categorized according to the I_{para}/I_{dia} threshold values of 0.8 and 0.6 for moderate PRE (yellow) and strong PRE (red), respectively. These thresholds are represented by horizontal dashed lines. Error bars were generated based on the signal-to-noise ratios. (B) Mapping PRE-affected probes onto the crystal structure of KRAS-GDP (PDB ID: 4DSU) in the arbitrary dimerization model that reflects our experimental conditions. Probes that show moderate and strong PREs are colored in orange and red, respectively, in the same way as in panel (A), and probes not substantially affected by PRE are colored in dark gray. Dotted lines represent PRE effects that arise from TEMPO conjugated to Sγ atoms of Cys118 (red) and Cys169 (blue) in the opposing FP-KRAS-GDP protomer.

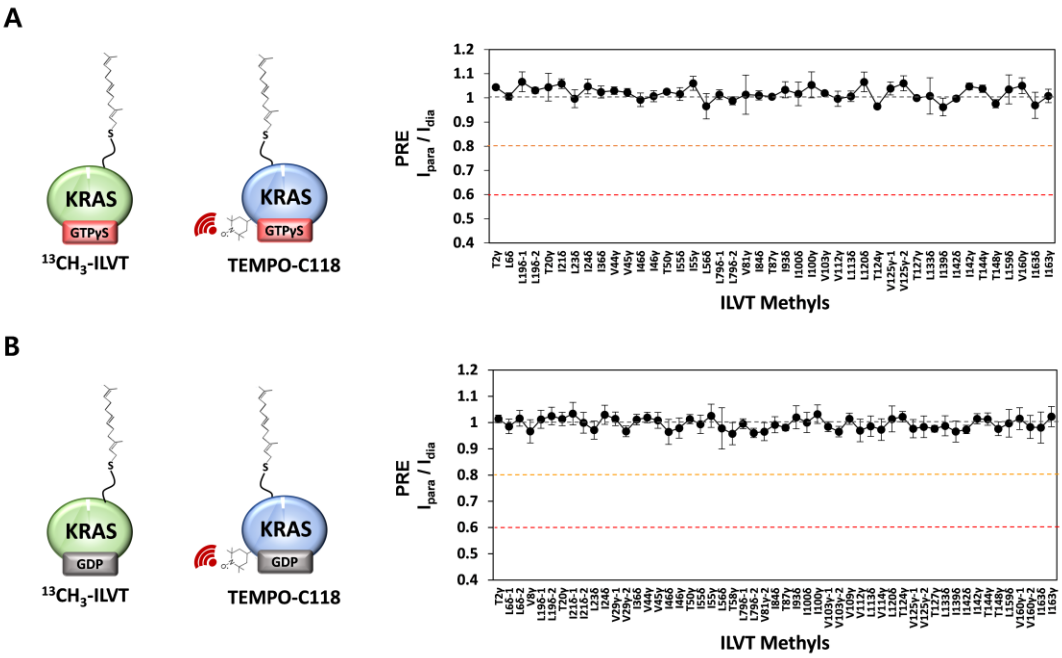

Figure S4. In the absence of a lipid bilayer, no PRE effects were observed between ^{13}C-labeled FP-KRAS and TEMPO-labeled FP-KRAS for either the GTPγS- (A) or GDP-loaded (B) states. Left panels illustrate the experimental design with [ILVT-^{13}C methyl]-labeled FP-KRAS and FP-KRAS bearing a TEMPO spin label at Cys118. Right panels show the plots of the intensity ratios of ILVT methyl peaks in the presence of paramagnetic versus diamagnetic (reduced) spin labels (I_{para}/I_{dia}).

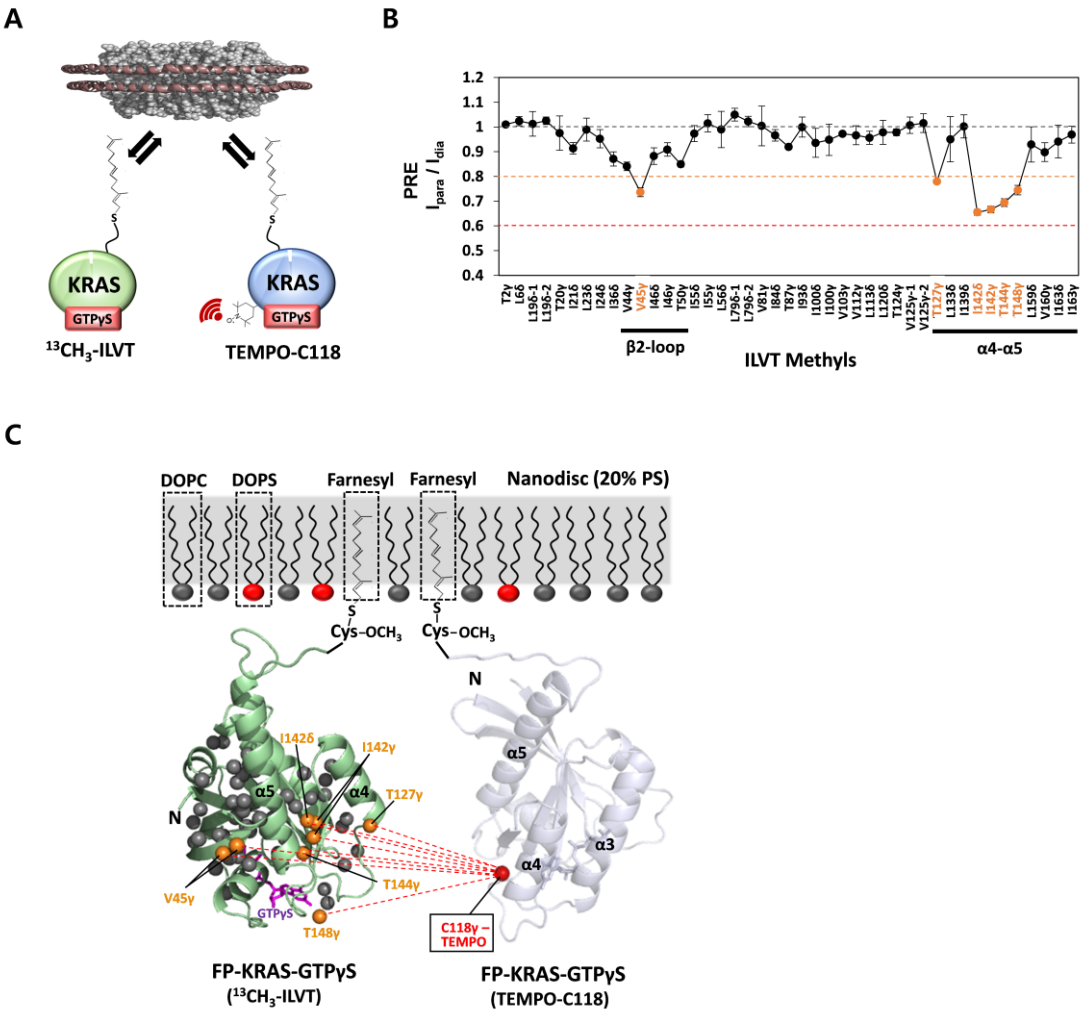

Figure S5. Intermolecular PRE effects between ^{13}C-labeled FP-KRAS-GTPγS and TEMPO-labeled FP-KRAS-GTPγS in the presence of nanodiscs. (A) Illustration of the experimental design with [ILVT-^{13}C methyl]-labeled FP-KRAS-GTPγS, TEMPO-labeled FP-KRAS-GTPγS, and nanodisc. (B) Intensity ratios of peaks in the presence of paramagnetic versus diamagnetic (reduced) spin labels (I_{para}/I_{dia}) for ILVT ^{13}C-methyl probes of FP-KRAS-GTPγS in the presence of nanodiscs upon addition of an equivalent amount of FP-KRAS-GTPγS bearing a TEMPO spin label at Cys118. The molar ratio of FP-KRAS-GTPγS per nanodisc leaflets was optimized as 10:1. (C) Mapping of PRE-broadened probes onto the crystal structure of GTPγS-bound KRAS (PDB ID: 4DSO) in the arbitrary dimerization model with TEMPO-labeled FP-KRAS-GTPγS and a nanodisc containing 20% PS. Red dotted lines represent intermolecular PRE effects from TEMPO conjugated to the Sγ atom of Cys118 in the opposing FP-KRAS-GTPγS protomer. In panel (B) and (C), NMR probes showing moderate PREs with $0.6 < I_{para}/I_{dia} < 0.8$ are colored in orange.

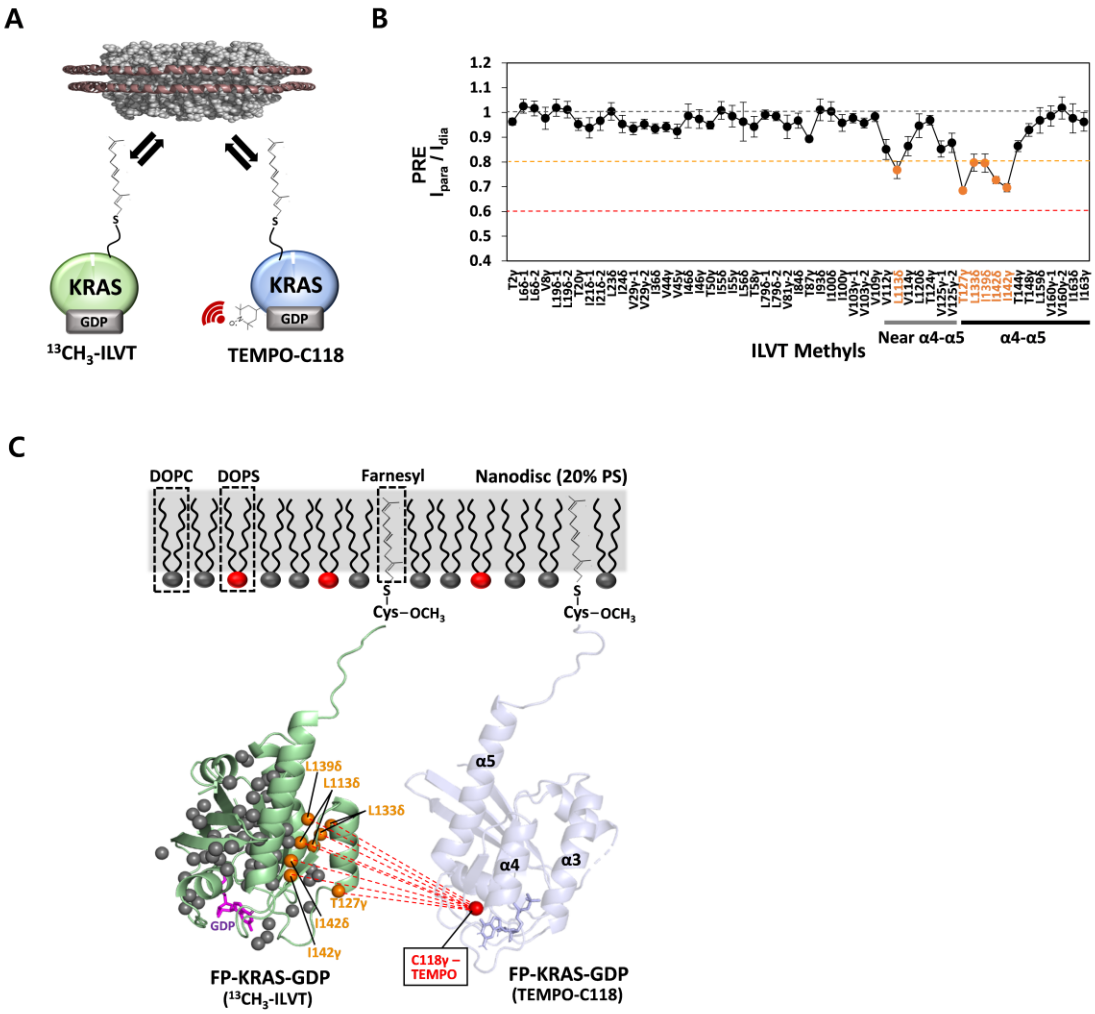

Figure S6. Intermolecular PRE effects between ^{13}C-labeled FP-KRAS-GDP and TEMPO-labeled FP-KRAS-GDP in the presence of nanodiscs. (A) Illustration of the experimental design with [ILVT-^{13}C methyl]-labeled FP-KRAS-GDP, TEMPO-labeled FP-KRAS-GDP, and nanodisc. (B) Intensity ratios of peaks in the presence of paramagnetic versus diamagnetic (reduced) spin labels (I_{para}/I_{dia}) for ILVT ^{13}C-methyl probes of FP-KRAS-GDP in the presence of nanodiscs upon addition of an equivalent amount of FP-KRAS-GDP bearing a TEMPO spin label at Cys118. The molar ratio of FP-KRAS-GDP per nanodisc leaflet was optimized as 10:1. (C) Mapping of PRE-broadened probes onto the crystal structure of GDP-bound KRAS (PDB ID: 4DSU) in the arbitrary dimerization model with TEMPO-labeled FP-KRAS-GDP and the nanodisc containing 20% PS. Red dotted lines represent intermolecular PRE effects from TEMPO conjugated to the Sγ atom of Cys118 in the opposing FP-KRAS-GDP protomer. In panel (B) and (C), NMR probes showing moderate PREs with $0.6 < I_{para}/I_{dia} < 0.8$ are colored in orange.

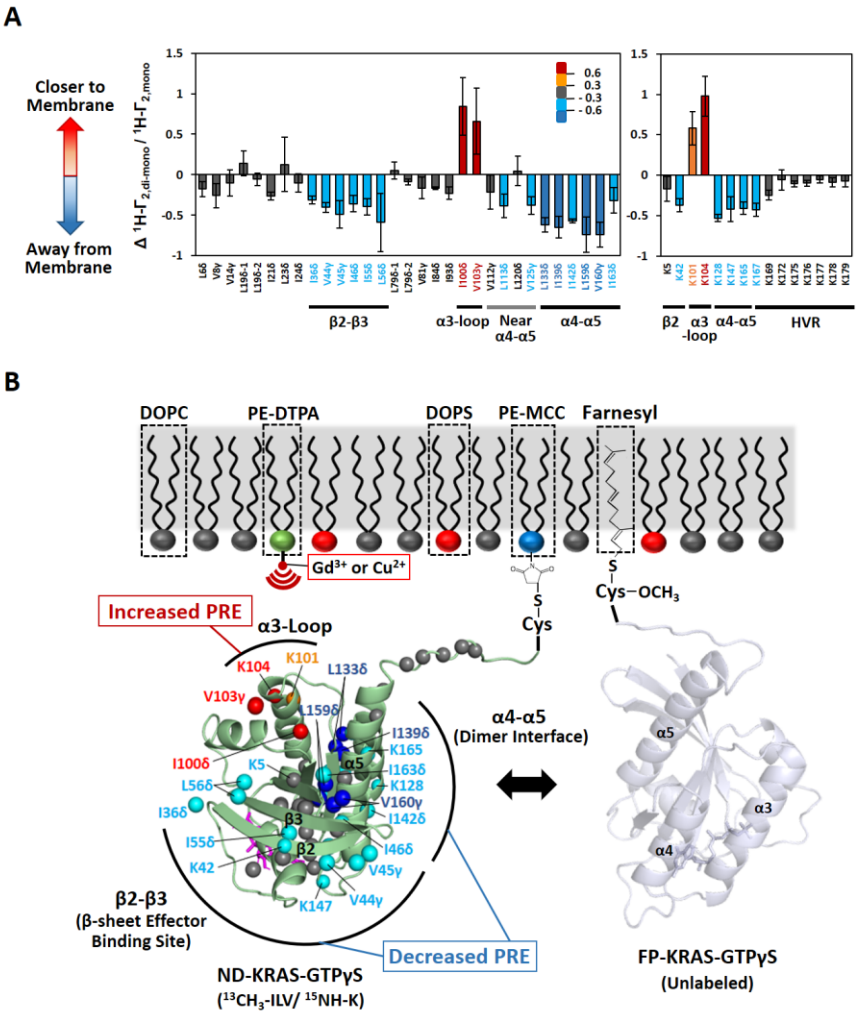

Figure S7. Dimerization-induced changes in PRE effects on KRAS-GTPγS from membrane-associated spin labels. (A) Relative changes by residue of ^{1}H transverse PRE rates (Δ^{1}H-$\Gamma_{2,\text{di-mono}}/^{1}$H-$\Gamma_{2,\text{mono}}$) of MC-KRAS-GTPγS ILV methyls and Lys amides upon addition of FP-KRAS-GTPγS. Gd^{3+}- or Cu^{2+}-conjugated lipids were incorporated in nanodiscs for methyl and amide experiments, respectively. Positive and negative values represent gain and loss of PRE effects, respectively. Probes with PRE changes are grouped and colored according to the threshold values of Δ^{1}H-$\Gamma_{2,\text{di-mono}}/^{1}$H-$\Gamma_{2,\text{mono}}$: large PRE gain (red) with ratio of > 0.6, moderate PRE gain (orange) with 0.3 < ratio < 0.6, moderate PRE loss (cyan) with - 0.6 < ratio < - 0.3, and large PRE loss (blue) with ratio of < - 0.6. (B) Mapping of dimerization-induced PRE changes onto the structure of KRAS-GTPγS in the arbitrary dimerization model. Probes are color-coded according to PRE change as in (A), and probes with no PRE changes are colored in dark gray. Regions that undergo gain or loss of PRE effects from are indicated. This model is built using a crystal structure of GTPγS-bound KRAS (PDB ID: 4DSO) and a nanodisc containing 20% phosphatidylserine (PS) and 5% Gd^{3+}- or Cu^{2+}-chelated PE-DTPA.

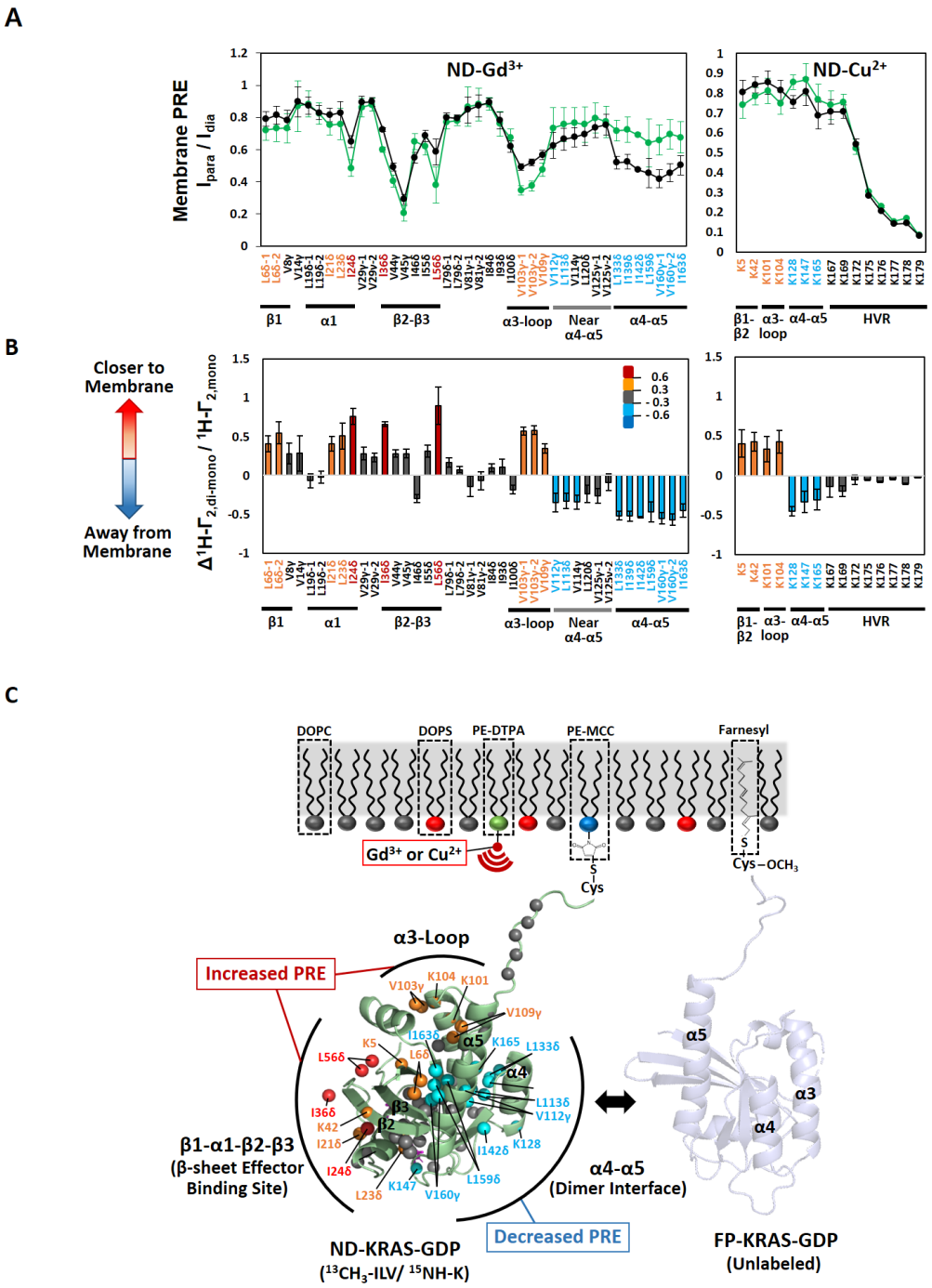

Figure S8. Dimerization-induced changes in membrane PRE effects on KRAS-GDP from membrane-associated spin labels. Panels A and B are presented in the same way as Figure 3 and S7a, respectively. In panel (C), probes with PRE changes are mapped onto the crystal structure of GDP-bound KRAS (PDB ID: 4DSU)

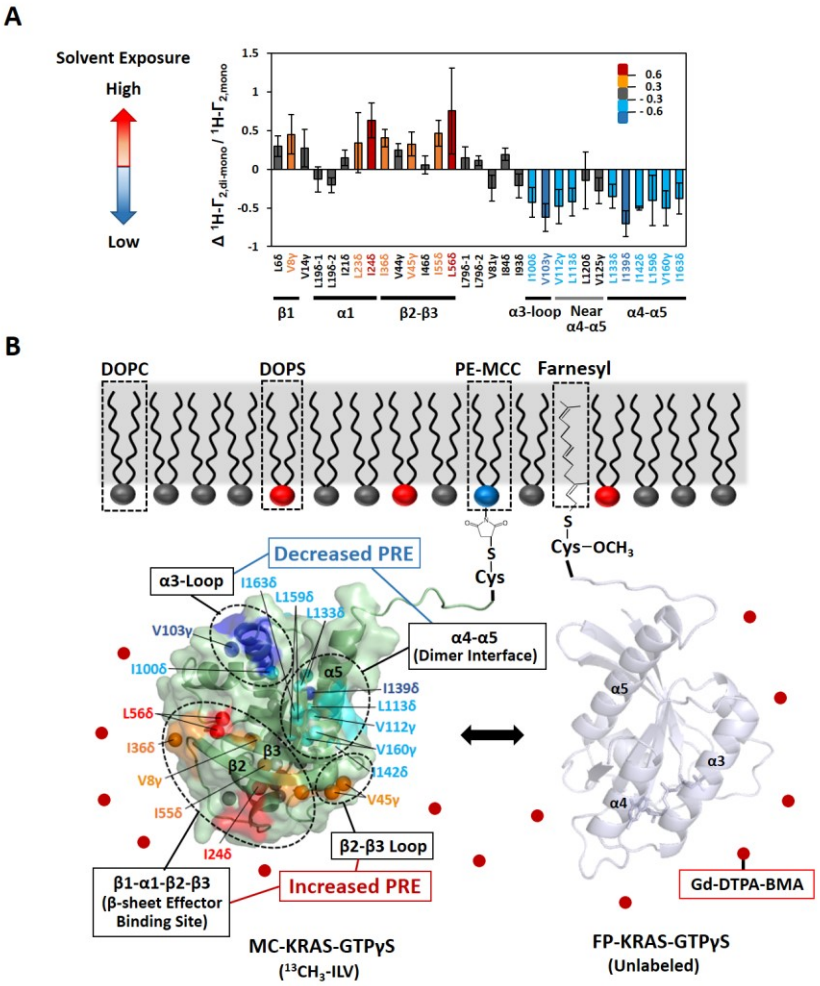

Figure S9. Dimerization-induced changes in solvent PRE effects on KRAS-GTPγS. (A) Relative changes of ^{1}H transverse PRE rates (Δ^{1}H-$\Gamma_{2,\text{di-mono}}$/^{1}H-$\Gamma_{2,\text{mono}}$) of MC-KRAS-GTPγS ILV methyls upon addition of FP-KRAS-GTPγS in the presence of Gd-DTPA-BMA. Probes with solvent PRE changes are grouped and colored according to the threshold values of Δ^{1}H-$\Gamma_{2,\text{di-mono}}$/^{1}H-$\Gamma_{2,\text{mono}}$: large PRE gain (red) with ratio of > 0.6, a moderate PRE gain (orange) with 0.3 < ratio < 0.6, moderate PRE loss (cyan) with - 0.6 < ratio < - 0.3, and large PRE loss (blue) with ratio of < - 0.6. (B) Mapping solvent PRE changes onto the surface of MC-KRAS-GTPγS in the arbitrary dimerization model. Probes with dimerization-induced solvent PRE changes are color-coded in the same way as (A), and probes that do not exhibit substantial PRE changes are colored dark gray. For clarity, the surfaces of residues with PRE changes and flanking residues (i ± 1) are shown in the same color. Regions that undergo gain and loss of solvent PRE effects from Gd-DTPA-BMA (depicted as red circles) are indicated. The dimerization model was constructed using the crystal structure of GTPγS-bound KRAS (PDB ID: 4DSO) and a nanodisc containing 20% phosphatidylserine (PS). Gd-DTPA-BMA is assumed to collide randomly with solvent-exposed sites of MC-KRAS-GTPγS.

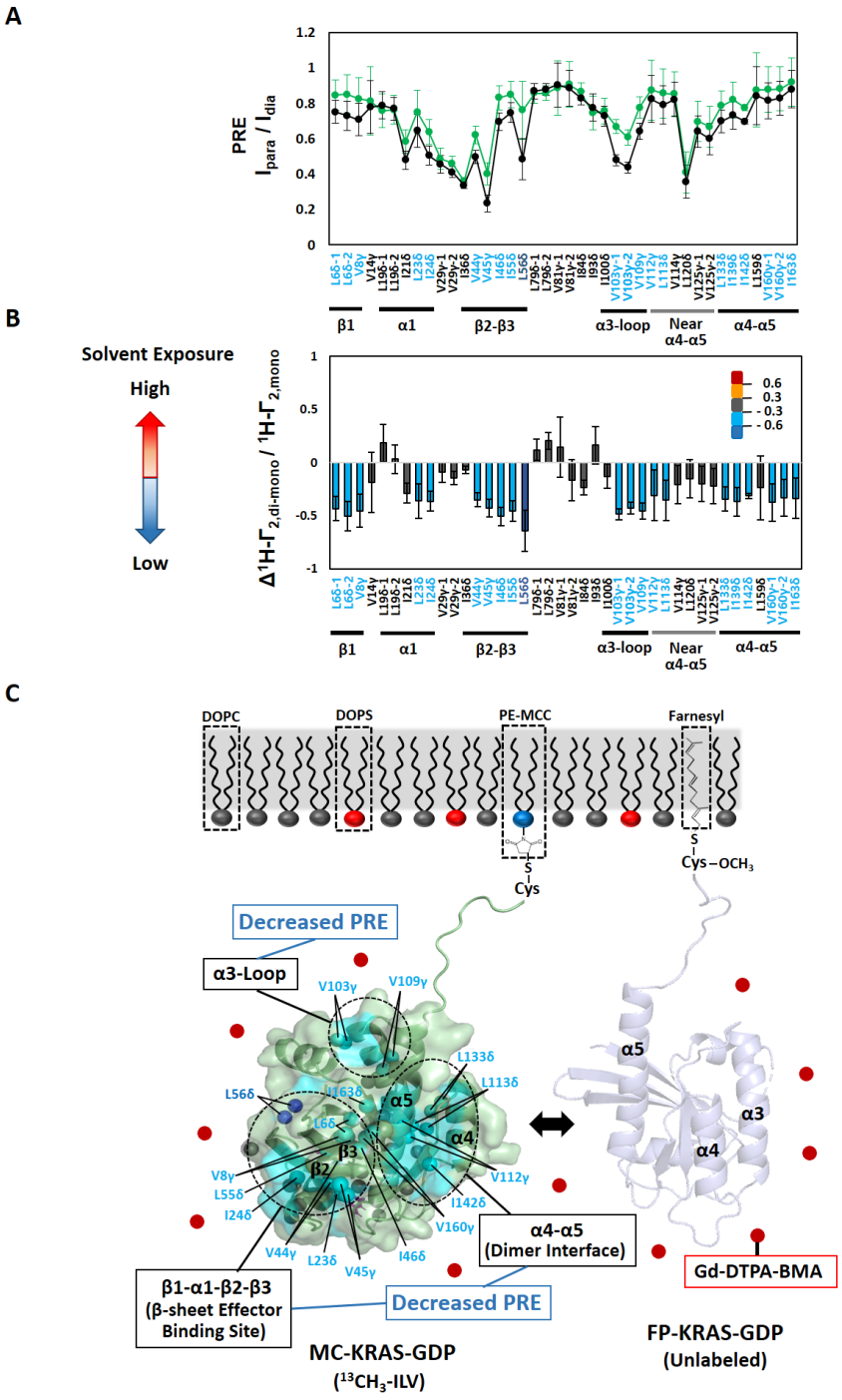

Figure S10. Dimerization-induced changes in solvent PRE effects on KRAS-GDP. Panels (A) and (B) are presented as in Figure 3 and Figure S9a, respectively. In panel (C), probes with dimerization-induced changes in PRE effects are mapped onto the crystal structure of GDP-bound KRAS (PDB ID: 4DSU).

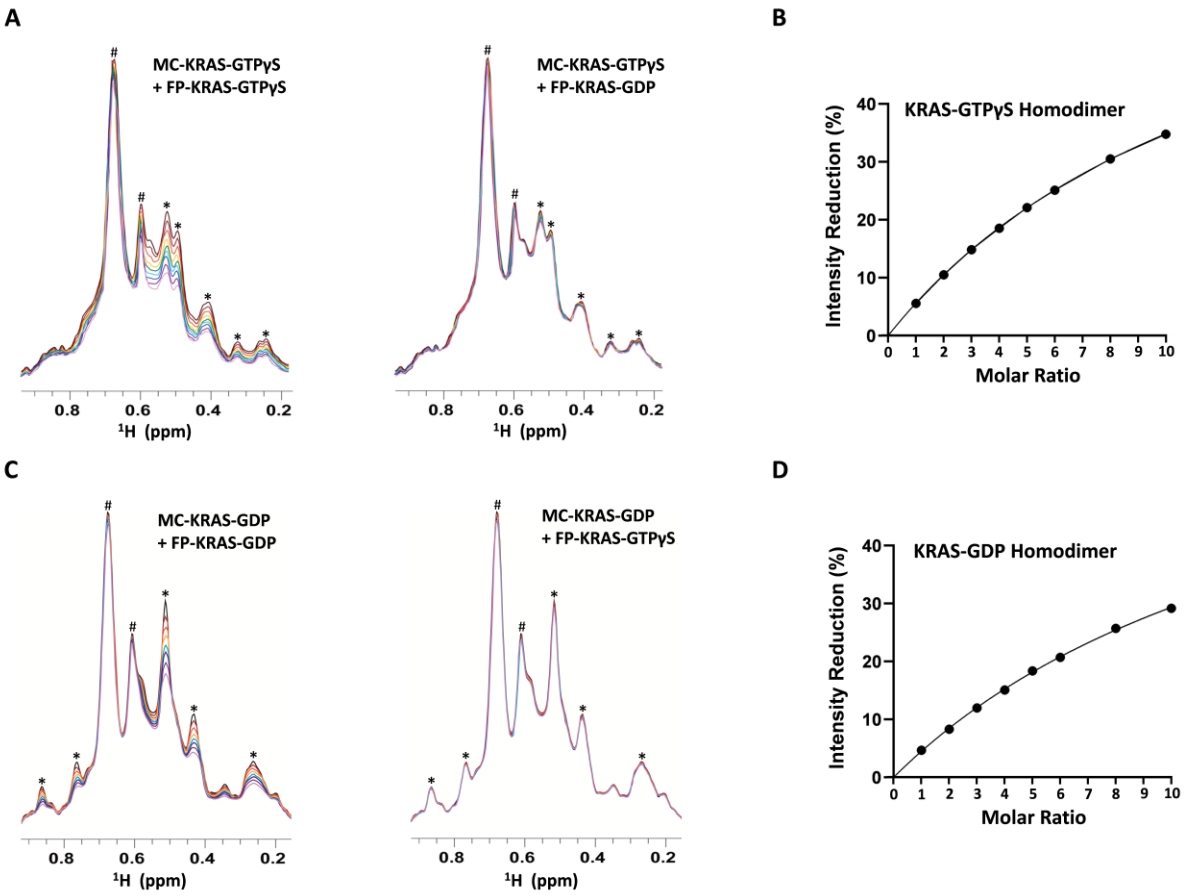

Figure S11. Apparent dissociation constant (K_D) for KRAS dimerization on nanodiscs in both the GTPγS- and GDP-bound states. (A, C) One-dimensional ^{1}H-^{13}C TROSY spectra for ILV ^{13}C-methyl protons of 40 μM nanodisc-tethered MC-KRAS-GTPγS (A) and MC-KRAS-GDP (C) in the presence of increasing molar equivalents (1, 2, 3, 4, 5, 6, 8, and 10) of FP-KRAS-GTPγS or FP-KRAS-GDP. * indicates MC-KRAS peaks that are used for K_D estimation. # indicates peaks derived from the aliphatic methyl protons of lipids in nanodiscs, which were identified in the spectrum of the nanodisc alone and excluded from the analysis. (B, D) Plots of the average relative intensity reductions (%) of MC-KRAS peaks versus the molar equivalents of FP-KRAS added. The titration data fit well to one-site binding models with apparent K_D values of 530 μM for the KRAS-GTPγS homodimer and 610 μM for the KRAS-GDP homodimer. The curve-fitting was performed using GraphPad Prism version 8 for Windows, GraphPad Software, La Jolla California USA, www.graphpad.com.

A

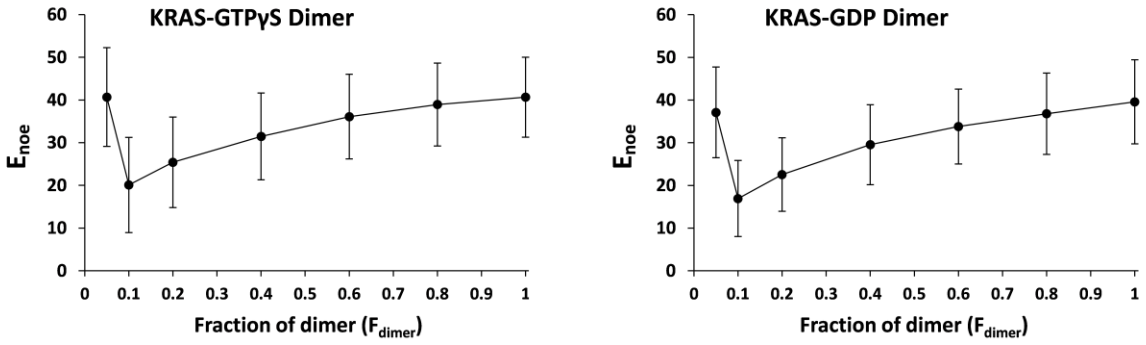

B

$$E_{noe} = \begin{cases} (d-L)^2 & \text{if } d < L \\ 0 & \text{if } L < d < U \\ (d-U)^2 & \text{if } U < d < U + 1 \\ 2(d-U) - 1 & \text{if } d > U + 1 \end{cases}$$

Figure S12. Optimization of KRAS dimer models in both the GTPγS- and GDP-bound states using the sets of distance restraints calculated using variable values for the fraction of KRAS that is dimeric (F_{dimer}). (A) NOE distance restraint potential (E_{noe}) of the 200 lowest Haddock-score structures versus fraction of dimer (F_{dimer}). Seven F_{dimer} values, 0.05, 0.1, 0.2, 0.4, 0.6, 0.8, and 1.0, were used as inputs for the calculation of the corresponding sets of PRE-derived distances in equation 2 in the Methods and Materials section. (B) Conditional formulas to calculate E_{noe}. "L" and "U" represent the lower and upper limits of distance restraints, respectively, and "d" indicates the corresponding distance in the final HADDOCK models.

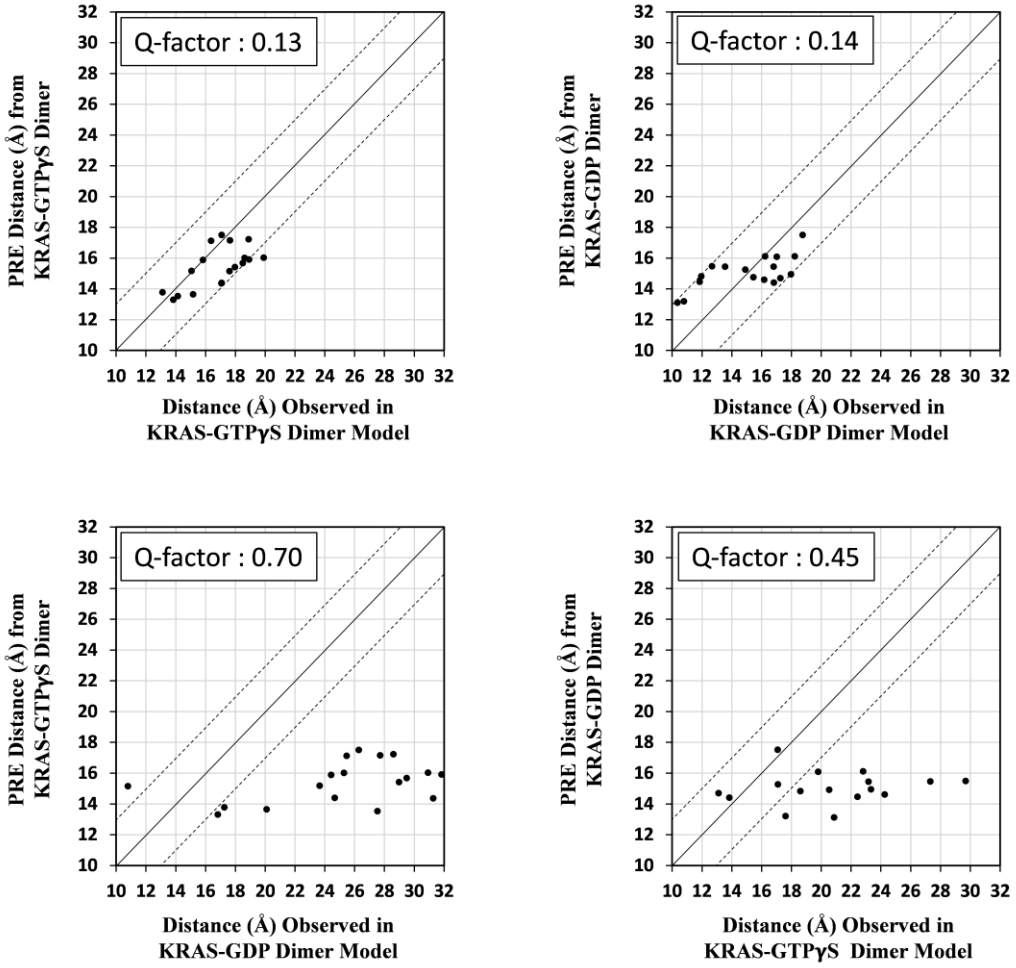

Figure S13. Correlation between distance derived from TEMPO-PRE experiments and distance observed in the reference structure of the KRAS dimer in both the GTPγS- and GDP-bound states. These distances are described in Table S2. Q-factor indicated is a measure of agreement between PRE-derived and model distances (see equation 4 in the Material and Methods section). The diagonal solid line represents that PRE-derived distance is equal to model distance, with upper and lower bounds of ± 3.0 Å, as indicated by dotted lines.

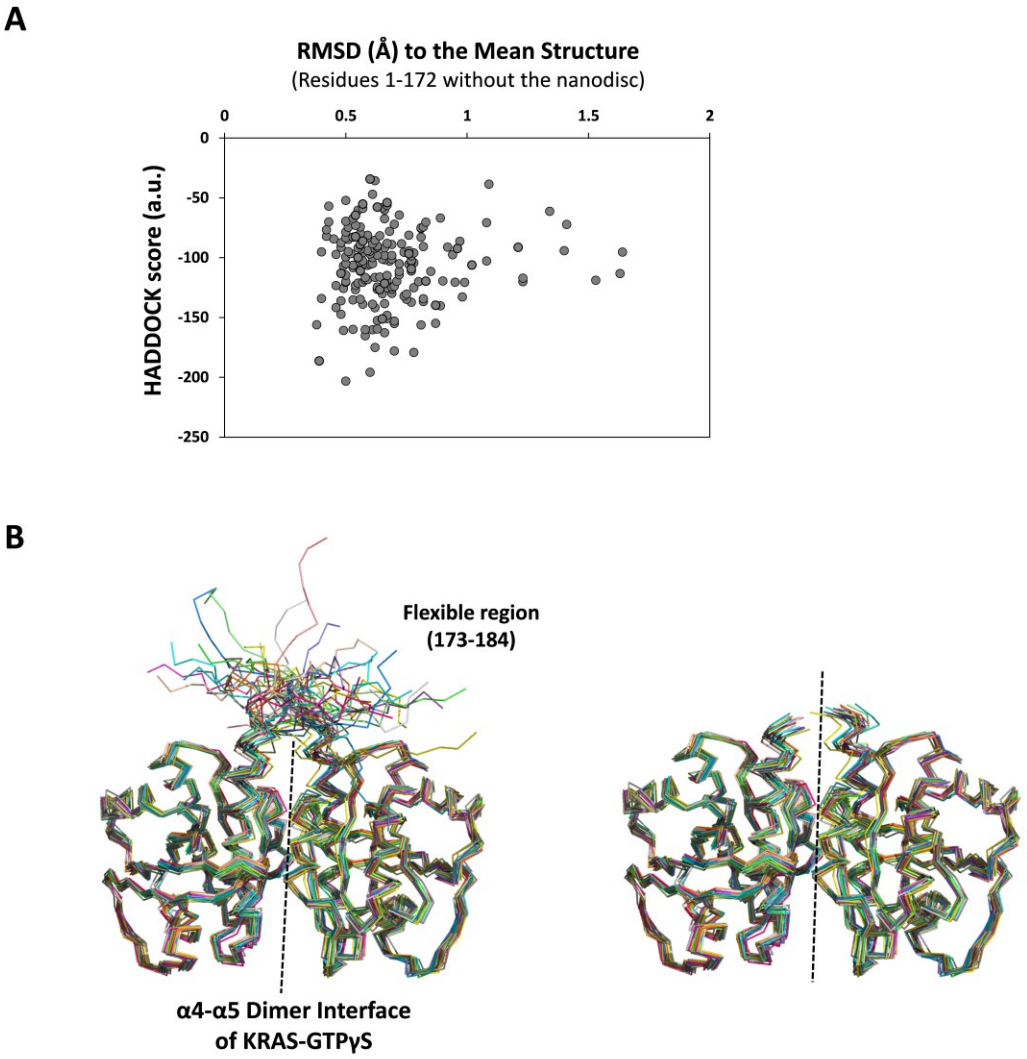

Figure S14. The lowest HADDOCK-score models of the GTPγS-bound KRAS homodimer. (A) Plot of HADDOCK scores of the 200 final structures of the GTPγS-bound KRAS homodimer (residues 1-172) versus RMSD values to the mean structure. (B) Overlay of the 20 lowest HADDOCK-score structures of the GTPγS-bound KRAS homodimer with (left) and without (right) the C-terminal flexible region (residues 173-184).

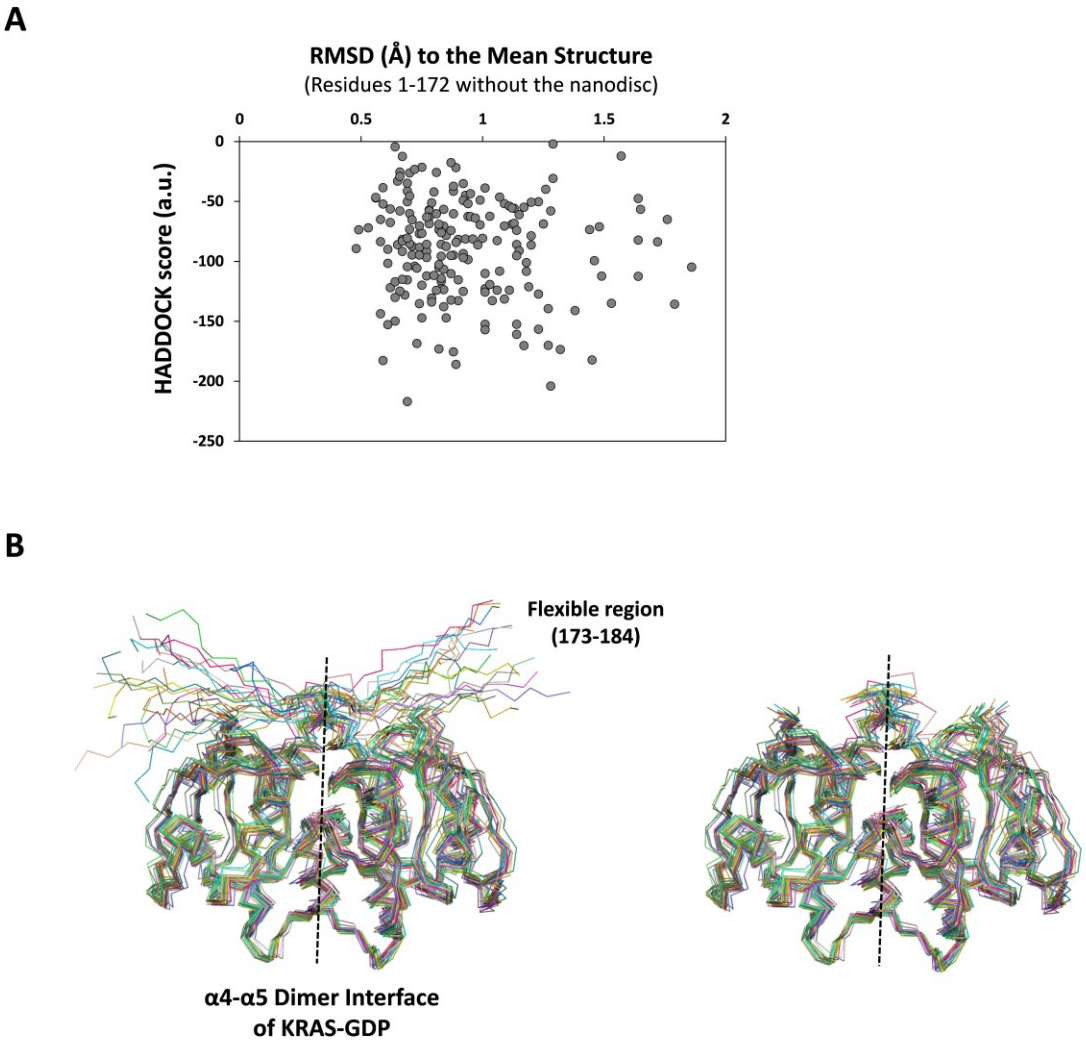

Figure S15. The lowest HADDOCK-score models of the GDP-bound KRAS homodimer. (A) Plot of HADDOCK scores of the 200 final structures of the GDP-bound KRAS homodimer (Residues 1-172) versus RMSD values to the mean structure. (B) Overlay of the 20 lowest HADDOCK-score structures of the GDP-bound KRAS homodimer with (left) and without (right) the C-terminal flexible region (residues 173-184).

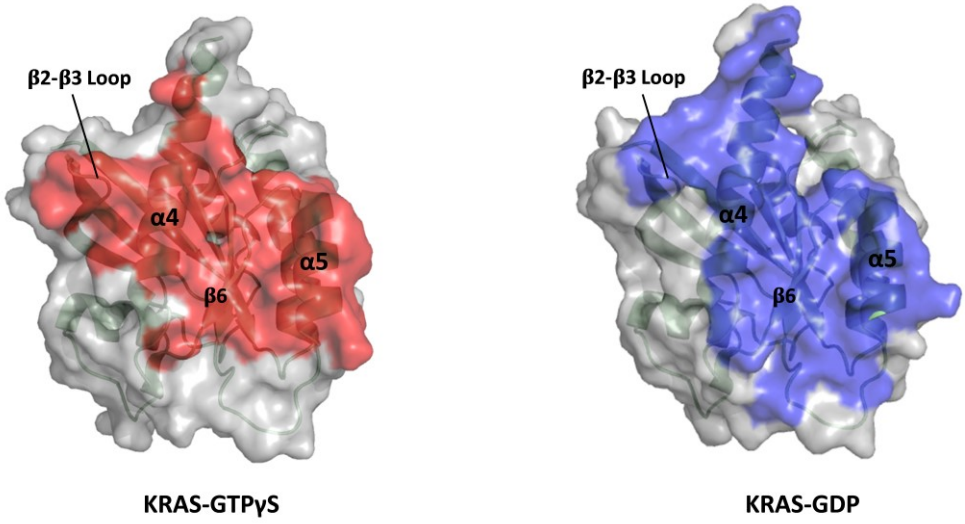

Figure S16. Dimer interfaces mapped onto the reference structures of the KRAS homodimers (residues 1-172) in the GTPγS- and GDP-bound states.

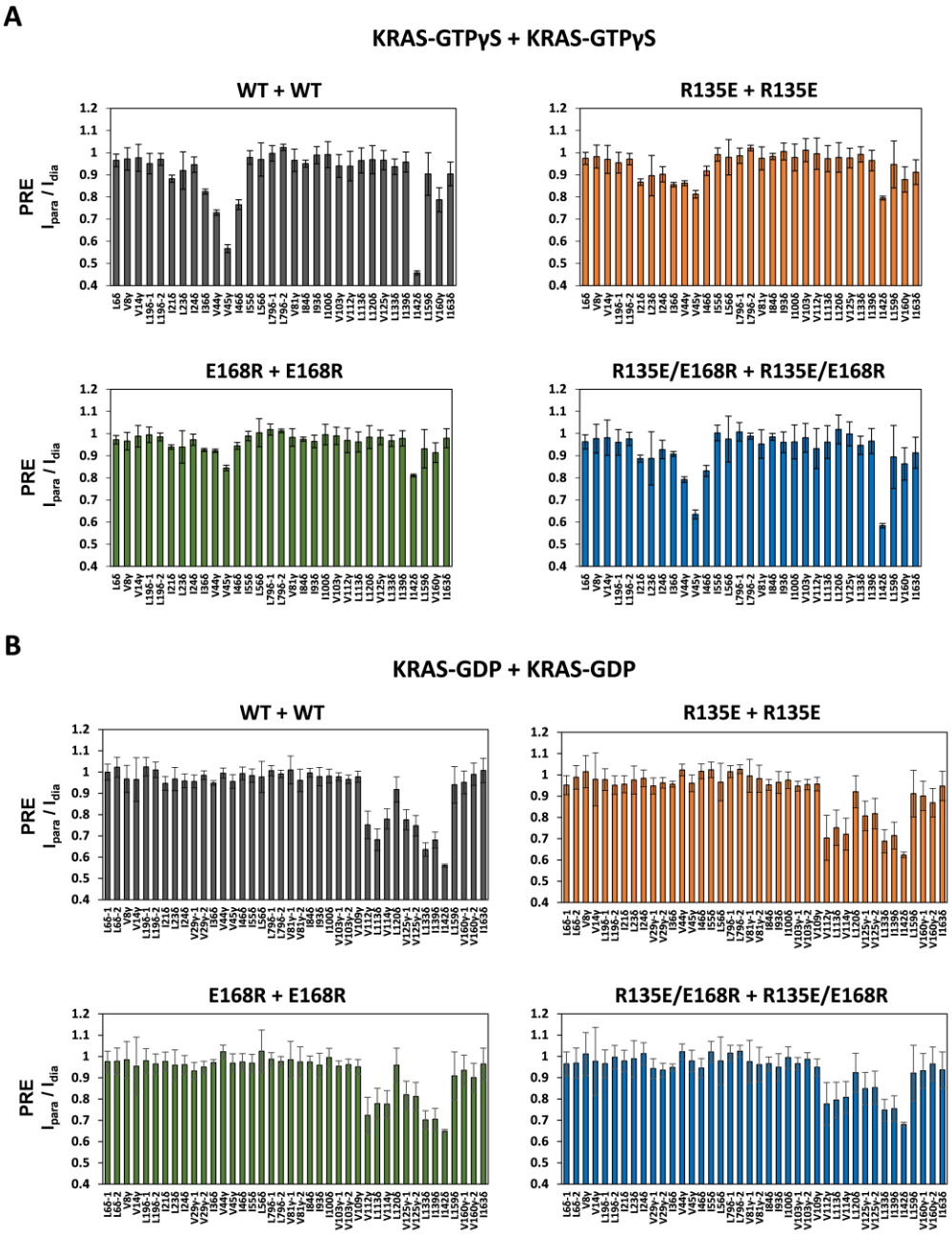

Figure S17. Effects of mutations of ion pairs identified within the KRAS-GTPγS homodimer interface on intermolecular PRE effects of KRAS-GTPγS (A) and KRAS-GDP (B). Relative intensity ratios of paramagnetic to diamagnetic (reduced) peaks (I_{para}/I_{dia}) for ILV ^{13}C-methyl probes of wild and mutant types of MC-KRAS (WT, R135E, E168R, and R135E/E168R) were calculated in the presence of equivalent amounts of FP-KRAS (same mutation and nucleotide) bearing a TEMPO tag at Cys118.

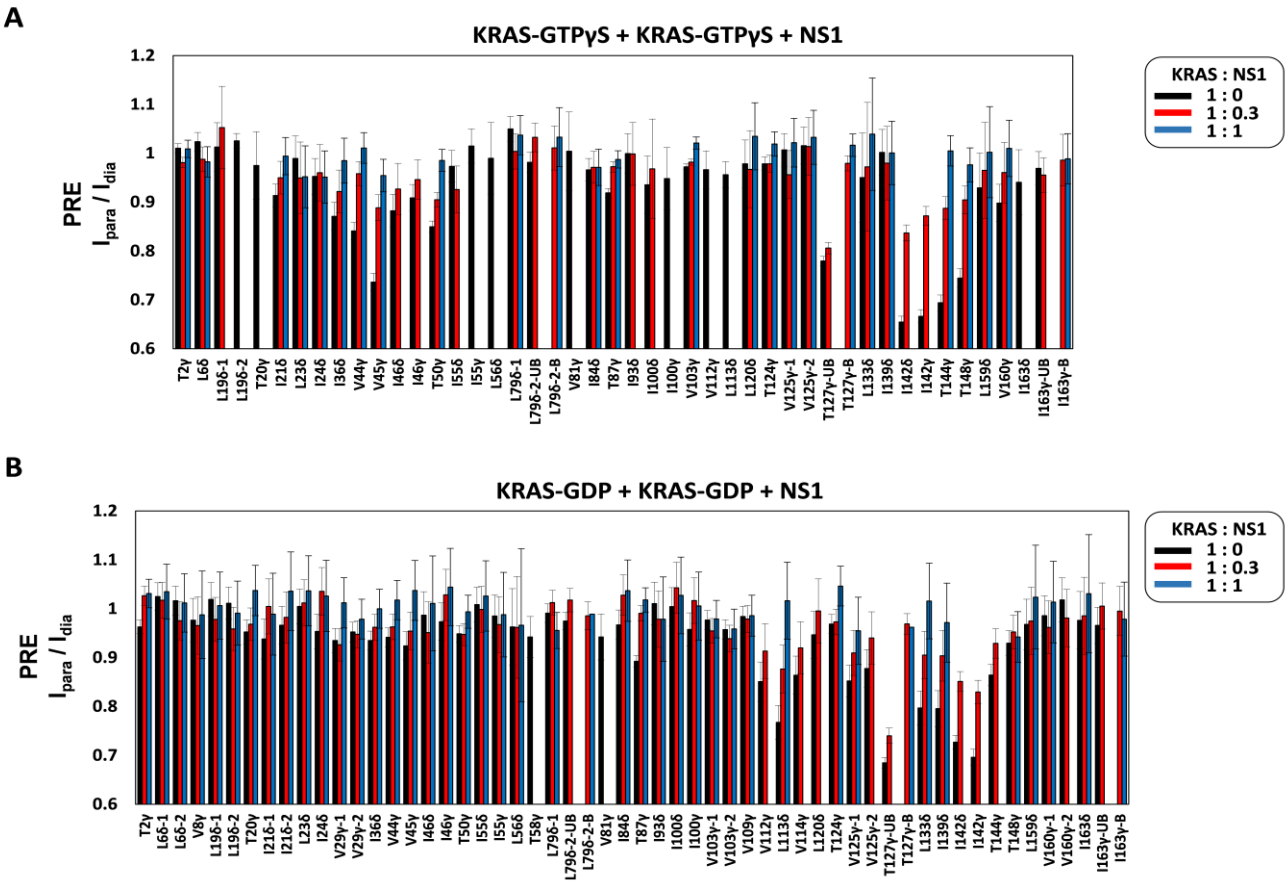

Figure S18. Intermolecular PRE effects within homodimeric interfaces of KRAS-GTPγS (A) and KRAS-GDP (B) on nanodiscs in the presence of increasing amounts of the monobody NS1. Relative intensity ratios of paramagnetic to diamagnetic (reduced) peaks (I_{para}/I_{dia}) for ILVT ^{13}C-methyl probes of FP-KRAS were calculated in the presence of equivalent amounts of FP-KRAS bearing a TEMPO tag at Cys118. These values were obtained in titrations with 0.3 and 1 molar equivalents of the NS1 monobody to FP-KRAS. The molar ratio of FP-KRAS to one leaflet of the nanodisc was 10:1. "UB" and "B" following L79δ -2, T127γ and I163γ on the x-axis represent distinct peaks for NS1-unbound and -bound states of KRAS, respectively.

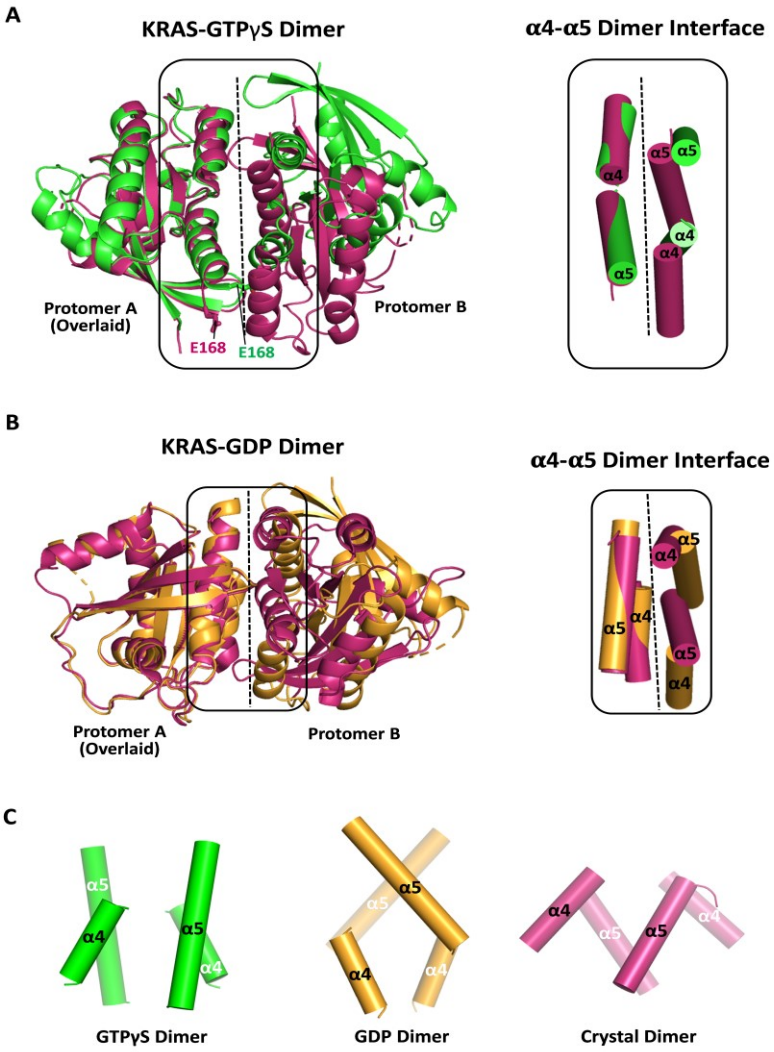

Figure S19. Structural comparison between models of full-length KRAS dimers on the membrane versus crystallographic contacts observed for truncated KRAS in both the GTPγS and GDP states. (A, B) PRE-derived structures of the full-length KRAS dimers on the membrane compared with the crystal structures of truncated KRAS GTPase domain 'dimers' (PDB IDs: 5VQ6 for GTPγS state and 5W22 for GDP state). For clarity, only the GTPase-domains (residues 1-168) of PRE-derived structures are shown. PRE-derived dimers in the GTPγS- and GDP-bound states are colored in green (A, GTPγS) and orange (B, GDP), respectively, while the crystallographic dimers are colored violet. One protomer in each KRAS dimer is overlaid to clearly show the different arrangements of the opposing protomers. The different relative orientations of the α4 and α5 helices at the dimer interface are highlighted in the cylindrical models at the right. Panel (A) illustrates the different orientations of the side chains of E168 in the overlaid protomers. (C) Frontal views of the relative orientations between the interfacial α4 and α5 helices of membrane-associated versus crystallographic KRAS dimers.

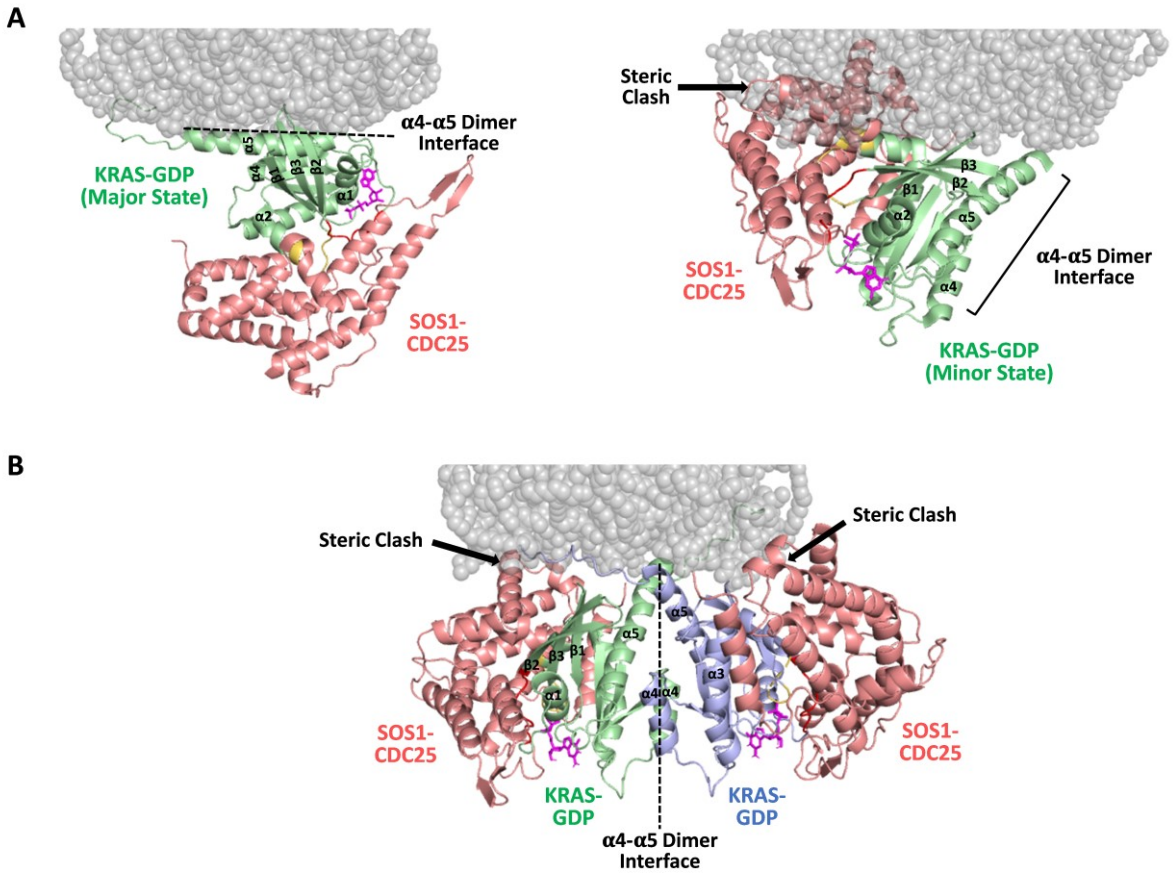

C

	KRAS-GDP Monomer (Major State)	KRAS-GDP Monomer (Minor State)	KRAS-GDP Dimer
SOS1-CDC25 Binding Site (β-interface)	Exposed	Occluded	Occluded
α4-α5 Dimer Interface (α-interface)	Occluded	Exposed	Occluded

Figure S20. Structural models of the SOS1 catalytic domain (SOS1-CDC25) in complex with the monomeric and homodimeric forms of membrane-associated KRAS-GDP. (A) Binding of SOS1-CDC25 to GDP-bound KRAS monomer is compatible with the membrane orientation of the the major state (left), but not in the minor state (right). Arrow represents a steric clash between SOS1-CDC25 and the membrane lipids. These complex models are reconstituted based on NMR-derived structures of membrane-associated KRAS monomers in "exposed" (PDB ID: 2MSC) and "occluded" states (PDB ID: 2MSD) and the crystal structure of the HRAS-SOS1 complex (PDB ID: 1BKD). (B) Orientation of the GDP-bound KRAS homodimer on the membrane is not compatible with SOS1-CDC25 binding. Binding of SOS1-CDC25 to the KRAS-GDP homodimer would make a steric clash with the membrane. (C) Accessibility of the SOS1-CDC25 binding site (β-interface) and the α4-α5 dimer interface (α-interface) in the monomeric and dimeric forms of GDP-bound KRAS are designated as "occluded" or "exposed".

A

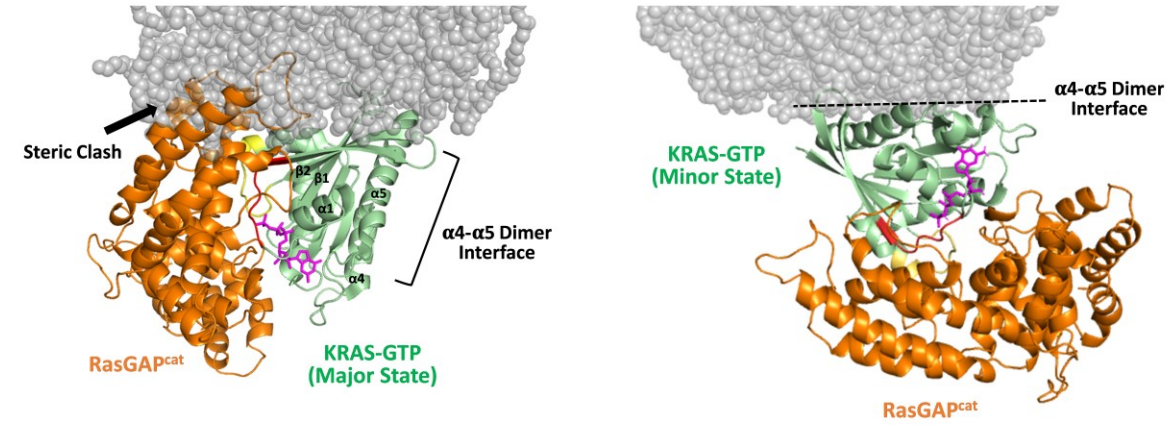

B

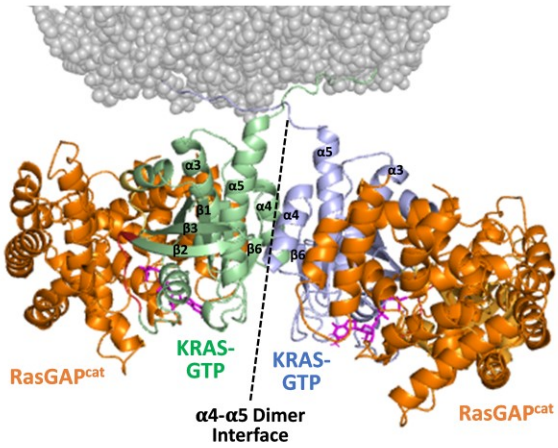

C

	KRAS-GTP Monomer (Major State)	KRAS-GTP Monomer (Minor State)	KRAS-GTP Dimer
RasGAP^{cat} Binding Site (β-interface)	Occluded	Exposed	Exposed
α4-α5 Dimer Interface (α-interface)	Exposed	Occluded	Occluded

Figure S21. Structural models of the P120 RasGAP catalytic domain (RasGAP^{cat}) in complex with monomeric and dimeric forms of membrane-associated KRAS-GTP. (A) Binding of RasGAP^{cat} to membrane-associated KRAS is compatible with the orientation of the GTP-bound KRAS monomer in the minor state (right), but not in the major state (left). Arrow represents a steric clash between RasGAP^{cat} and the membrane lipids. These complex models are reconstituted based on NMR-derived structures of membrane-associated KRAS monomers in "exposed" (PDB ID: 2MSC) and "occluded" states (PDB ID: 2MSD) and the crystal structure of the HRAS-RasGAP complex (PDB ID: 1WQ1). (B) Orientation of the GTPγS-bound KRAS homodimer on the membrane is compatible with RasGAP^{cat} binding. (C) Accessibility of the RasGAP^{cat} binding site (β-interface) and the α4-α5 dimer interface (α-interface) in the monomeric and dimeric forms of GTP analogue-bound KRAS are designated as "occluded" or "exposed".

5. Supporting Tables

Table S1. Statistics for the 20 lowest HADDOCK-score models of membrane-anchored KRAS homodimers in both the GTPγS- and GDP-bound states

KRAS-GTPγS Homodimer	
PRE-derived Distance Restraints	
For KRAS dimer interface	
Number of PRE restraints (± 3.0 Å)	36
Number of non-PRE restraints (only a lower limit)	198
For KRAS dimer-membrane interface	
Number of PRE restraints (- 10.0 Å/ + 0.0 Å)	20
Energy Statistics	
HADDOCK score (a.u.)	-166 ± 15
Van der Waals energy (kcal/mol)	-77 ± 15
Electrostatic energy (kcal/mol)	-728 ± 124
Desolvation energy (kcal/mol)	42 ± 13
Restraints violation energy (kcal/mol)	141 ± 61
Total buried surface area (Å^2)	3461 ± 361
KRAS-GDP Homodimer	
PRE-derived Distance Restraints	
For KRAS dimer interface	
Number of PRE restraints (± 3.0 Å)	38
Number of non-PRE restraints (only a lower limit)	244
For KRAS dimer-membrane interface	
Number of PRE restraints (- 10.0 Å/ + 0.0 Å)	32
Energy Statistics	
HADDOCK score (a.u.)	-169 ± 18
Van der Waals energy (kcal/mol)	-98 ± 15
Electrostatic energy (kcal/mol)	-782 ± 109
Desolvation energy (kcal/mol)	73 ± 15
Restraints violation energy (kcal/mol)	114 ± 72
Total buried surface area (Å^2)	4696 ± 458

Table S2. Violation analysis of PRE-derived distance restraints from GTPγS- and GDP-bound KRAS in the reference structure of the KRAS dimer in each nucleotide state.

KRAS-GTPγS Homodimer Model									PRE Distance (Å) from KRAS-GTPγS	Result[#]
Chain	Residue Number	Atom Name	Chain	Residue Number	Atom Name	Distance (Å)	d_{eff}*	Average Distance (Å)		
B	118	SG	C	44	CG1	20.2	18.1	18.0	15.4 ± 3.0	S
B	118	SG	C	44	CG2	20.5				
C	118	SG	B	44	CG1	19.9	17.8			
C	118	SG	B	44	CG2	20.1				
B	118	SG	C	45	CG1	18.7	17.0	17.1	14.4 ± 3.0	S
B	118	SG	C	45	CG2	19.5				
C	118	SG	B	45	CG1	20.6	17.2			
C	118	SG	B	45	CG2	18.4				
B	118	SG	C	46	CD1	18.4		18.5	15.7 ± 3.0	S
C	118	SG	B	46	CD1	18.6				
B	118	SG	C	142	CD1	14.4		13.8	13.3 ± 3.0	S
C	118	SG	B	142	CD1	13.3				
B	118	SG	C	160	CG1	20.9	18.4	18.6	16.0 ± 3.0	S
B	118	SG	C	160	CG2	20.4				
C	118	SG	B	160	CG1	21.3	18.8			
C	118	SG	B	160	CG2	21.0				
B	118	SG	C	127	CG2	17.7		17.6	15.2 ± 3.0	S
C	118	SG	B	127	CG2	17.5				
B	118	SG	C	142	CG2	13.5		13.1	13.8 ± 3.0	S
C	118	SG	B	142	CG2	12.7				
B	118	SG	C	144	CG2	14.7		15.2	13.7 ± 3.0	S
C	118	SG	B	144	CG2	15.6				
B	118	SG	C	148	CG2	17.4		17.1	14.4 ± 3.0	S
C	118	SG	B	148	CG2	16.7				
B	169	CG	C	113	CD1	18.8	15.8	15.8	15.9 ± 3.0	S
B	169	CG	C	113	CD2	17.0				
C	169	CG	B	113	CD1	18.6	15.8			

C	169	CG	B	113	CD2	17.1				
B	169	CG	C	125	CG1	22.1	20.5	19.9	16.0 ± 3.0	V
B	169	CG	C	125	CG2	24.2				
C	169	CG	B	125	CG1	21.0	19.3			
C	169	CG	B	125	CG2	22.6				
B	169	CG	C	133	CD1	14.9	13.8	14.1	13.5 ± 3.0	S
B	169	CG	C	133	CD2	16.4				
C	169	CG	B	133	CD1	15.7	14.4			
C	169	CG	C	133	CD2	16.8				
B	169	CG	C	139	CD1	14.9		15.1	15.2 ± 3.0	S
C	169	CG	B	139	CD1	15.2				
B	169	CG	C	128	N	19.0		18.9	15.9 ± 3.0	S
C	169	CG	B	128	N	18.8				
B	169	CG	C	176	N	16.2		16.4	17.1 ± 3.0	S
C	169	CG	B	176	N	16.6				
B	169	CG	C	177	N	17.9		17.1	17.5 ± 3.0	S
C	169	CG	B	177	N	16.3				
B	169	CG	C	178	N	17.9		17.6	17.2 ± 3.0	S
C	169	CG	B	178	N	17.4				
B	169	CG	C	179	N	19.6		18.9	17.2 ± 3.0	S
C	169	CG	B	179	N	18.18				

KRAS-GDP Homodimer Model									**PRE Distance (Å) from KRAS-GTPγS**	**Result[#]**
Chain	**Residue Number**	**Atom Name**	**Chain**	**Residue Number**	**Atom Name**	**Distance (Å)**	***d_{eff}****	**Average Distance (Å)**		
B	118	SG	C	44	CG1	32.7	28.8	29.0	15.4 ± 3.0	V
B	118	SG	C	44	CG2	32.0				
C	118	SG	B	44	CG1	32.8	29.1			
C	118	SG	B	44	CG2	32.6				
B	118	SG	C	45	CG1	33.3	30.3	31.3	14.4 ± 3.0	V
B	118	SG	C	45	CG2	34.9				
C	118	SG	B	45	CG1	35.7	32.2			
C	118	SG	B	45	CG2	36.7				

B	118	SG	C	46	CD1	29.3		29.5	15.7 ± 3.0	V
C	118	SG	B	46	CD1	29.7				
B	118	SG	C	142	CD1	17.5		16.8	13.3 ± 3.0	V
C	118	SG	B	142	CD1	16.2				
B	118	SG	C	160	CG1	28.5	25.3	25.3	16.0 ± 3.0	V
B	118	SG	C	160	CG2	28.3				
C	118	SG	B	160	CG1	29.0	25.3			
C	118	SG	B	160	CG2	27.9				
B	118	SG	C	127	CG2	10.2		10.8	15.2 ± 3.0	V
C	118	SG	B	127	CG2	11.4				
B	118	SG	C	142	CG2	17.0		17.3	13.8 ± 3.0	V
C	118	SG	B	142	CG2	17.5				
B	118	SG	C	144	CG2	19.8		20.1	13.7 ± 3.0	V
C	118	SG	B	144	CG2	20.4				
B	118	SG	C	148	CG2	25.3		24.7	14.4 ± 3.0	V
C	118	SG	B	148	CG2	24.0				
B	169	CG	C	113	CD1	28.1	24.9	24.4	15.9 ± 3.0	V
B	169	CG	C	113	CD2	27.7				
C	169	CG	B	113	CD1	27.1	24.0			
C	169	CG	B	113	CD2	26.7				
B	169	CG	C	125	CG1	34.4	31.4	30.9	16.0 ± 3.0	V
B	169	CG	C	125	CG2	36.3				
C	169	CG	B	125	CG1	33.4	30.5			
C	169	CG	B	125	CG2	35.1				
B	169	CG	C	133	CD1	31.2	27.4	27.5	13.5 ± 3.0	V
B	169	CG	C	133	CD2	30.5				
C	169	CG	B	133	CD1	31.4	27.6			
C	169	CG	C	133	CD2	30.6				
B	169	CG	C	139	CD1	23.8		23.7	15.2 ± 3.0	V
C	169	CG	B	139	CD1	23.5				
B	169	CG	C	128	N	32.4		31.8	15.9 ± 3.0	V
C	169	CG	B	128	N	31.3				

B	169	CG	C	176	N	23.3		25.5	17.1 ± 3.0	V
C	169	CG	B	176	N	27.6				
B	169	CG	C	177	N	23.7		26.3	17.5 ± 3.0	V
C	169	CG	B	177	N	28.9				
B	169	CG	C	178	N	24.4		27.7	17.2 ± 3.0	V
C	169	CG	B	178	N	31.0				
B	169	CG	C	179	N	23.6		28.6	17.2 ± 3.0	V
C	169	CG	B	179	N	33.62				

KRAS-GDP Homodimer Model									**PRE Distance (Å) from KRAS-GDP**	**Result[#]**
Chain	**Residue Number**	**Atom Name**	**Chain**	**Residue Number**	**Atom Name**	**Distance (Å)**	d_{eff}*	**Average Distance (Å)**		
B	118	SG	C	112	CG1	19.6	18.0	18.2	15.3 ± 3.0	S
B	118	SG	C	112	CG2	21.1				
C	118	SG	B	112	CG1	19.7	18.3			
C	118	SG	B	112	CG2	21.6				
B	118	SG	C	113	CD1	19.3	15.9	15.8	14.9 ± 3.0	S
B	118	SG	C	113	CD2	16.9				
C	118	SG	B	113	CD1	19.2	15.7			
C	118	SG	B	113	CD2	16.7				
B	118	SG	C	114	CG1	20.5	18.1	18.7	17.5 ± 3.0	S
B	118	SG	C	114	CG2	20.1				
C	118	SG	B	114	CG1	21.9	19.4			
C	118	SG	B	114	CG2	21.7				
B	118	SG	C	125	CG1	17.1	16.1	16.2	16.1 ± 3.0	S
B	118	SG	C	125	CG2	19.5				
C	118	SG	B	125	CG1	17.5	16.4			
C	118	SG	B	125	CG2	19.8				
B	118	SG	C	133	CD1	18.2	16.3	16.2	14.6 ± 3.0	S
B	118	SG	C	133	CD2	18.4				
C	118	SG	B	133	CD1	17.9	16.1			
C	118	SG	B	133	CD2	18.1				
B	118	SG	C	139	CD1	18.0		18.0	15.0 ± 3.0	S

C	118	SG	B	139	CD1	18.0				
B	118	SG	C	142	CD1	17.5		16.8	14.4 ± 3.0	S
C	118	SG	B	142	CD1	16.2				
B	118	SG	C	128	N	10.3		10.3	13.1 ± 3.0	S
C	118	SG	B	128	N	10.4				
B	118	SG	C	127	CG2	10.2		10.8	13.2 ± 3.0	S
C	118	SG	B	127	CG2	11.4				
B	118	SG	C	142	CG2	17.0		17.3	14.7 ± 3.0	S
C	118	SG	B	142	CG2	17.5				
B	169	CG	C	45	CG1	13.6	12.9	12.7	15.5 ± 3.0	S
B	169	CG	C	45	CG2	16.0				
C	169	CG	B	45	CG1	13.2	12.5			
C	169	CG	B	45	CG2	15.5				
B	169	CG	C	46	CD1	14.6		13.5	15.5 ± 3.0	S
C	169	CG	B	46	CD1	12.5				
B	169	CG	C	159	CD1	19.9	18.1	17.0	16.1 ± 3.0	S
B	169	CG	C	159	CD2	20.8				
C	169	CG	B	159	CD1	17.6	16.0			
C	169	CG	B	159	CD2	18.3				
B	169	CG	C	160	CG1	13.6	12.9	11.8	14.5 ± 3.0	S
B	169	CG	C	160	CG2	15.9				
C	169	CG	B	160	CG1	11.5	10.8			
C	169	CG	B	160	CG2	13.1				
B	169	CG	C	163	CD1	17.8		16.8	15.5 ± 3.0	S
C	169	CG	B	163	CD1	15.8				
B	169	CG	C	165	N	12.1		11.9	14.8 ± 3.0	S
C	169	CG	B	165	N	11.8				
B	169	CG	C	167	N	15.2		14.9	15.3 ± 3.0	S
C	169	CG	B	167	N	14.6				
B	169	CG	C	169	N	15.1		15.4	14.8 ± 3.0	S
C	169	CG	B	169	N	15.8				
B	169	CG	C	172	N	17.6		18.2	16.1 ± 3.0	S

C	169	CG	B	172	N	18.9				
KRAS-GTPγS Homodimer Model									**PRE Distance (Å) from KRAS-GDP**	**Result[#]**
Chain	**Residue Number**	**Atom Name[*]**	**Chain**	**Residue Number**	**Atom Name**	**Distance (Å)**	***d_{eff}****	**Average Distance (Å)**		
B	118	SG	C	112	CG1	18.5	16.9	17.1	15.3 ± 3.0	S
B	118	SG	C	112	CG2	19.5				
C	118	SG	B	112	CG1	19.0	17.3			
C	118	SG	B	112	CG2	19.8				
B	118	SG	C	113	CD1	23.4	20.4	20.5	14.9 ± 3.0	V
B	118	SG	C	113	CD2	22.5				
C	118	SG	B	113	CD1	23.8	20.6			
C	118	SG	B	113	CD2	22.6				
B	118	SG	C	114	CG1	18.7	16.5	17.1	17.5 ± 3.0	S
B	118	SG	C	114	CG2	18.3				
C	118	SG	B	114	CG1	19.8	17.7			
C	118	SG	B	114	CG2	19.9				
B	118	SG	C	125	CG1	24.7	22.7	22.8	16.1 ± 3.0	V
B	118	SG	C	125	CG2	26.4				
C	118	SG	B	125	CG1	24.8	23.0			
C	118	SG	B	125	CG2	27.1				
B	118	SG	C	133	CD1	27.7	24.0	24.3	14.6 ± 3.0	V
B	118	SG	C	133	CD2	26.4				
C	118	SG	B	133	CD1	28.2	24.5			
C	118	SG	B	133	CD2	26.8				
B	118	SG	C	139	CD1	23.3		23.3	15.0 ± 3.0	V
C	118	SG	B	139	CD1	23.4				
B	118	SG	C	142	CD1	14.4		13.8	14.4 ± 3.0	S
C	118	SG	B	142	CD1	13.3				
B	118	SG	C	128	N	20.9		20.9	13.1 ± 3.0	V
C	118	SG	B	128	N	20.9				
B	118	SG	C	127	CG2	17.7		17.6	13.2 ± 3.0	V
C	118	SG	B	127	CG2	17.5				

B	118	SG	C	142	CG2	13.5		13.1	14.7 ± 3.0	S
C	118	SG	B	142	CG2	12.7				
B	169	CG	C	45	CG1	32.4	29.5	29.7	15.5 ± 3.0	V
B	169	CG	C	45	CG2	33.9				
C	169	CG	B	45	CG1	33.9	29.9			
C	169	CG	B	45	CG2	33.2				
B	169	CG	C	46	CD1	27.4		27.3	15.5 ± 3.0	V
C	169	CG	B	46	CD1	27.2				
B	169	CG	C	159	CD1	21.1	19.7	19.8	16.1 ± 3.0	V
B	169	CG	C	159	CD2	23.6				
C	169	CG	B	159	CD1	21.3	19.9			
C	169	CG	B	159	CD2	23.7				
B	169	CG	C	160	CG1	25.0	22.5	22.4	14.5 ± 3.0	V
B	169	CG	C	160	CG2	25.4				
C	169	CG	B	160	CG1	25.0	22.4			
C	169	CG	B	160	CG2	25.4				
B	169	CG	C	163	CD1	23.2		23.2	15.5 ± 3.0	V
C	169	CG	B	163	CD1	23.1				
B	169	CG	C	165	N	18.6		18.6	14.8 ± 3.0	V
C	169	CG	B	165	N	18.6				
B	169	CG	C	167	N	19.2		19.2	15.3 ± 3.0	V
C	169	CG	B	167	N	19.3				
B	169	CG	C	169	N	17.4		17.4	14.8 ± 3.0	S
C	169	CG	B	169	N	17.5				
B	169	CG	C	172	N	19.4		19.4	16.1 ± 3.0	V
C	169	CG	B	172	N	19.4				

*An effective distance (d_{eff}) for ambiguous interactions was calculated with the following formula: $d_{eff} = \sum_{i=1}^{N_{atoms}} (\frac{1}{d_i^6})^{-\frac{1}{6}}$ where N_{atoms} indicates all atoms that are involved in ambiguous interactions.

"S" and "V" represent satisfaction and violation, respectively, of PRE distance restraints in the structure of the KRAS homodimer in each nucleotide state.

Table S3. Intermolecular interactions within the dimer interface of the 20 lowest HADDOCK-score models of the KRAS homodimer in the GTPγS -bound state.

Model	Chain	Residue Number	Residue Name	Atom Name	Chain	Residue Number	Residue Name	Atom Name	Distance* (Å)	Ion Pair#
1	B	131	GLN	OE1	C	161	ARG	HH12	2.1	
	B	131	GLN	OE1	C	161	ARG	HH21	1.9	
	B	131	GLN	HE22	C	154	ASP	OD1	1.7	
	B	135	ARG	HH21	C	47	ASP	OD1	1.8	O
	B	161	ARG	HH12	C	131	GLN	OE1	2.0	
	B	168	GLU	OE2	C	135	ARG	HH11	2.0	O
	B	177	LYS	HZ1	C	173	ASP	OD2	1.6	O
	B	181	SER	OG	C	176	LYS	HZ2	2.1	
2	B	132	ASP	OD1	C	164	ARG	HH12	2.3	O
	B	135	ARG	HH11	C	168	GLU	OE1	2.4	O
	B	135	ARG	HH12	C	168	GLU	OE2	1.9	O
	B	154	ASP	OD1	C	131	GLN	HE21	1.8	
	B	161	ARG	HH12	C	131	GLN	OE1	2.2	
	B	168	GLU	OE1	C	135	ARG	HH11	1.8	O
	B	173	ASP	OD1	C	184	LYS	HZ1	1.6	O
3	B	47	ASP	OD1	C	135	ARG	HH22	1.7	O
	B	131	GLN	OE1	C	161	ARG	HH12	2.1	
	B	131	GLN	OE1	C	161	ARG	HH21	2.2	
	B	131	GLN	HE22	C	154	ASP	OD1	1.8	
	B	135	ARG	HH11	C	168	GLU	OE1	1.7	O
	B	154	ASP	OD1	C	131	GLN	HE22	1.7	
	B	178	LYS	HZ1	C	173	ASP	OD1	1.8	O
	B	180	LYS	HZ1	C	105	ASP	OD2	1.8	O
4	B	107	GLU	OE1	C	179	LYS	HZ1	1.6	O
	B	107	GLU	OE1	C	184	LYS	HZ3	2.2	O
	B	107	GLU	OE2	C	184	LYS	HZ3	1.7	O
	B	108	ASP	OD1	C	175	LYS	HZ2	2.4	O
	B	108	ASP	OD1	C	175	LYS	HZ3	2.4	O
	B	108	ASP	OD2	C	175	LYS	HZ3	1.7	O
	B	131	GLN	OE1	C	161	ARG	HH12	2.4	

	B	132	ASP	OD1	C	164	ARG	HH11	2.2	O
	B	135	ARG	HH12	C	168	GLU	OE2	1.9	O
	B	154	ASP	OD2	C	131	GLN	HE22	2.1	
	B	161	ARG	HH12	C	131	GLN	OE1	2.2	
	B	161	ARG	HH21	C	131	GLN	OE1	2.4	
	B	168	GLU	OE1	C	135	ARG	HH12	1.9	O
	B	168	GLU	OE1	C	136	SER	HG	1.9	
5	B	131	GLN	OE1	C	161	ARG	HH21	2.0	
	B	131	GLN	HE22	C	154	ASP	OD1	2.0	
	B	135	ARG	HH12	C	168	GLU	OE2	1.9	O
	B	154	ASP	OD1	C	131	GLN	HE21	2.4	
	B	161	ARG	HH12	C	131	GLN	OE1	2.2	
	B	164	ARG	HH12	C	132	ASP	OD1	2.2	O
	B	168	GLU	OE2	C	135	ARG	HH11	1.6	O
	B	182	LYS	HZ1	C	136	SER	OG	2.5	
6	B	45	VAL	O	C	128	LYS	HZ3	1.8	
	B	131	GLN	OE1	C	161	ARG	HH12	2.3	
	B	131	GLN	HE22	C	154	ASP	OD1	1.8	
	B	135	ARG	HH11	C	168	GLU	OE1	1.7	O
	B	154	ASP	OD1	C	131	GLN	HE22	1.7	
	B	157	TYR	OH	C	128	LYS	HZ2	2.4	
	B	161	ARG	HH12	C	131	GLN	OE1	2.3	
	B	161	ARG	HH21	C	131	GLN	OE1	2.4	
	B	168	GLU	OE2	C	135	ARG	HH12	2.0	O
7	B	131	GLN	HE22	C	158	THR	OG1	1.9	
	B	135	ARG	HH22	C	168	GLU	OE1	1.7	O
	B	161	ARG	HH12	C	131	GLN	OE1	1.9	
	B	175	LYS	HZ3	C	173	ASP	OD1	2.1	O
	B	175	LYS	HZ3	C	173	ASP	O	2.4	
8	B	135	ARG	HH12	C	168	GLU	OE2	1.9	O
	B	135	ARG	HH22	C	47	ASP	OD2	1.6	O
	B	154	ASP	OD1	C	131	GLN	HE22	1.7	
	B	161	ARG	HH12	C	131	GLN	OE1	2.1	

	B	174	GLY	O	C	176	LYS	HZ1	2.5	
9	B	107	GLU	OE2	C	182	LYS	HZ1	1.7	O
	B	131	GLN	OE1	C	161	ARG	HH12	2.3	
	B	131	GLN	OE1	C	161	ARG	HH21	2.5	
	B	131	GLN	HE22	C	154	ASP	OD1	1.7	
	B	135	ARG	HH11	C	168	GLU	OE1	1.7	O
	B	154	ASP	OD1	C	131	GLN	HE22	1.7	
	B	161	ARG	HH12	C	131	GLN	OE1	2.1	
	B	161	ARG	HH21	C	131	GLN	OE1	2.2	
	B	168	GLU	OE1	C	135	ARG	HH11	2.5	O
	B	168	GLU	OE1	C	135	ARG	HH21	1.7	O
	B	168	GLU	OE2	C	135	ARG	HH11	1.9	O
	B	173	ASP	OD2	C	180	LYS	HZ1	1.7	
10	B	45	VAL	O	C	128	LYS	HZ3	1.9	
	B	91	GLU	OE2	C	184	LYS	HZ1	1.7	O
	B	108	ASP	OD2	C	175	LYS	HZ3	1.6	O
	B	136	SER	OG	C	177	LYS	HZ3	1.8	
	B	150	GLN	HE22	C	150	GLN	OE1	2.0	
	B	154	ASP	OD2	C	131	GLN	HE21	2.4	
	B	161	ARG	HH12	C	131	GLN	OE1	2.3	
	B	161	ARG	HH21	C	131	GLN	OE1	2.1	
	B	168	GLU	OE1	C	135	ARG	HH11	1.7	O
11	B	131	GLN	HE22	C	154	ASP	OD2	1.9	
	B	135	ARG	HH12	C	168	GLU	OE2	1.8	O
	B	154	ASP	OD1	C	131	GLN	HE22	1.7	
	B	161	ARG	HH21	C	131	GLN	OE1	1.9	
	B	168	GLU	OE1	C	135	ARG	HH12	1.8	O
	B	168	GLU	OE2	C	136	SER	HG	1.9	
	B	179	LYS	HZ2	C	107	GLU	OE1	1.6	O
	B	180	LYS	HZ2	C	108	ASP	OD1	1.7	O
	B	180	LYS	HZ2	C	108	ASP	OD2	2.4	O
	B	181	SER	HG	C	173	ASP	OD2	1.8	
12	B	131	GLN	OE1	C	161	ARG	HH12	2.5	

	B	131	GLN	HE22	C	154	ASP	OD1	1.8	
	B	135	ARG	HH21	C	168	GLU	OE1	1.7	O
	B	168	GLU	OE1	C	135	ARG	HH12	1.9	O
	B	173	ASP	OD2	C	182	LYS	HZ2	1.6	O
	B	173	ASP	O	C	182	LYS	HZ3	2.0	
13	B	108	ASP	OD2	C	175	LYS	HZ3	1.6	O
	B	131	GLN	OE1	C	161	ARG	HH12	2.2	
	B	135	ARG	HH12	C	168	GLU	OE1	1.7	O
	B	161	ARG	HH12	C	131	GLN	OE1	2.4	
14	B	131	GLN	HE22	C	154	ASP	OD1	1.9	
	B	131	GLN	HE22	C	154	ASP	OD2	2.3	
	B	135	ARG	HH11	C	168	GLU	OE1	1.6	O
	B	154	ASP	OD2	C	131	GLN	HE22	1.9	
	B	161	ARG	HH21	C	131	GLN	OE1	2.4	
	B	168	GLU	OE1	C	135	ARG	HH11	1.7	O
	B	181	SER	OG	C	175	LYS	HZ3	1.7	
	B	182	LYS	HZ2	C	173	ASP	OD1	2.5	O
	B	182	LYS	HZ2	C	173	ASP	OD2	1.6	O
	B	184	LYS	HZ3	C	170	MET	O	2.1	
15	B	131	GLN	HE22	C	154	ASP	OD2	1.8	
	B	135	ARG	HH22	C	47	ASP	OD2	1.9	O
	B	154	ASP	OD1	C	131	GLN	HE22	1.7	
	B	161	ARG	HH21	C	131	GLN	OE1	1.8	
	B	164	ARG	HH11	C	132	ASP	OD1	2.4	O
	B	168	GLU	OE1	C	135	ARG	HH11	1.8	O
16	B	98	GLU	OE2	C	179	LYS	HZ2	1.8	O
	B	101	LYS	HZ2	C	177	LYS	O	2.3	
	B	102	ARG	HH12	C	183	THR	OG1	2.3	
	B	107	GLU	OE2	C	177	LYS	HN	2.3	O
	B	108	ASP	OD1	C	175	LYS	HZ3	1.7	O
	B	131	GLN	HE22	C	154	ASP	OD1	2.3	
	B	131	GLN	HE22	C	154	ASP	OD2	2.4	
	B	135	ARG	HH11	C	168	GLU	OE1	1.7	O

	B	135	ARG	HH21	C	168	GLU	OE1	2.0	O
	B	154	ASP	OD2	C	131	GLN	HE22	1.7	
	B	168	GLU	OE1	C	135	ARG	HH11	1.6	O
17	B	131	GLN	OE1	C	161	ARG	HH21	2.3	
	B	135	ARG	HH11	C	168	GLU	OE1	1.9	O
	B	136	SER	HG	C	168	GLU	OE1	1.9	
	B	161	ARG	HE	C	131	GLN	OE1	2.0	
	B	161	ARG	HH22	C	131	GLN	OE1	2.1	
	B	164	ARG	O	C	135	ARG	HH22	1.8	
	B	173	ASP	OD1	C	182	LYS	HZ1	1.7	O
	B	176	LYS	HZ2	C	181	SER	O	2.4	
	B	180	LYS	O	C	178	LYS	HZ3	2.1	
	B	181	SER	O	C	178	LYS	HZ2	1.9	
	B	184	LYS	HZ3	C	107	GLU	O	2.1	
18	B	131	GLN	OE1	C	161	ARG	HH12	2.4	
	B	131	GLN	OE1	C	161	ARG	HH21	2.1	
	B	131	GLN	HE22	C	154	ASP	OD1	1.7	
	B	161	ARG	HH12	C	131	GLN	OE1	2.0	
	B	161	ARG	HH21	C	131	GLN	OE1	2.3	
	B	182	LYS	HZ1	C	173	ASP	O	2.2	
	B	182	LYS	HZ3	C	173	ASP	OD1	1.7	O
19	B	47	ASP	OD2	C	135	ARG	HH22	1.9	O
	B	106	SER	OG	C	183	THR	HG1	1.7	
	B	107	GLU	HN	C	183	THR	OG1	1.9	
	B	107	GLU	OE1	C	179	LYS	HZ2	1.6	O
	B	108	ASP	OD1	C	181	SER	HG	1.9	
	B	131	GLN	OE1	C	161	ARG	HH12	2.0	
	B	131	GLN	OE1	C	161	ARG	HH21	2.3	
	B	131	GLN	HE22	C	154	ASP	OD1	1.7	
	B	135	ARG	HH11	C	168	GLU	OE1	1.8	O
	B	154	ASP	OD1	C	131	GLN	HE22	2.5	
	B	154	ASP	OD2	C	131	GLN	HE22	2.0	
	B	175	LYS	HZ2	C	182	LYS	O	1.8	

	B	180	LYS	HZ2	C	173	ASP	OD2	1.7	O
20	B	131	GLN	OE1	C	161	ARG	HH12	2.3	
	B	131	GLN	OE1	C	161	ARG	HH21	2.2	
	B	131	GLN	HE22	C	154	ASP	OD1	1.7	
	B	154	ASP	OD2	C	131	GLN	HE22	2.0	
	B	161	ARG	HH12	C	131	GLN	OE1	2.2	
	B	161	ARG	HH21	C	131	GLN	OE1	2.0	
	B	173	ASP	OD1	C	180	LYS	HZ1	1.6	O

* Cutoff distance to define a hydrogen bond is 2.5 Å.

A hydrogen bond in an ion-pair interaction is indicated as “O”

Table S4. Intermolecular interactions within the dimer interface of the 20 lowest HADDOCK-score models of the KRAS homodimer in the GDP-bound state.

Model	Chain	Residue Number	Residue Name	Atom Name	Chain	Residue Number	Residue Name	Atom Name	Distance* (Å)	Ion Pair#
1	B	1	SER	HN	C	180	LYS	O	2.2	
	B	49	GLU	OE2	C	172	LYS	HZ1	1.6	O
	B	118	CYS	O	C	128	LYS	HZ1	2.1	
	B	131	GLN	HE22	C	143	GLU	OE2	1.8	
	B	132	ASP	OD1	C	150	GLN	HE21	1.9	
	B	161	ARG	HH22	C	162	GLU	OE1	1.9	O
	B	162	GLU	OE2	C	165	LYS	HZ3	1.6	O
	B	172	LYS	HZ3	C	49	GLU	OE1	1.6	O
2	B	49	GLU	OE1	C	172	LYS	HZ1	2.5	O
	B	128	LYS	HZ2	C	118	CYS	O	2.4	
	B	131	GLN	HE21	C	141	PHE	O	2.1	
	B	143	GLU	O	C	135	ARG	HE	2.4	
	B	143	GLU	O	C	135	ARG	HH22	2.1	O
	B	165	LYS	HZ3	C	162	GLU	OE2	1.6	O
3	B	49	GLU	OE1	C	172	LYS	HZ1	2.3	O
	B	49	GLU	OE2	C	172	LYS	HZ1	1.7	O
	B	131	GLN	HE22	C	143	GLU	OE2	1.8	
	B	132	ASP	OD1	C	150	GLN	HE21	2.1	
	B	143	GLU	OE2	C	131	GLN	HE22	1.8	
	B	162	GLU	OE2	C	165	LYS	HZ3	1.7	O
	B	172	LYS	HZ3	C	49	GLU	OE2	2.3	O
	B	176	LYS	HZ1	C	49	GLU	OE1	1.6	O
	B	176	LYS	HZ2	C	2	THR	OG1	1.6	
	B	176	LYS	HZ3	C	50	THR	O	2.5	
	B	178	LYS	HZ2	C	1	SER	OG	1.8	
4	B	1	SER	OG	C	176	LYS	HZ3	1.8	
	B	3	GLU	OE2	C	180	LYS	HZ1	1.6	O
	B	49	GLU	OE2	C	172	LYS	HZ1	1.7	O
	B	50	THR	OG1	C	176	LYS	HZ2	2.0	
	B	132	ASP	OD2	C	150	GLN	HE21	1.9	

	B	143	GLU	OE2	C	131	GLN	HE22	1.8	
	B	172	LYS	HZ1	C	49	GLU	OE1	1.7	O
	B	176	LYS	HZ2	C	1	SER	OG	1.9	
5	B	47	ASP	HN	C	177	LYS	O	2.5	
	B	47	ASP	O	C	175	LYS	HN	1.9	
	B	49	GLU	OE1	C	172	LYS	HZ3	1.6	O
	B	127	THR	OG1	C	131	GLN	HE22	2.0	
	B	132	ASP	OD2	C	150	GLN	HE21	2.0	
	B	135	ARG	HE	C	154	ASP	OD2	1.6	O
	B	143	GLU	O	C	135	ARG	HE	2.3	O
	B	154	ASP	OD1	C	178	LYS	HZ1	1.7	O
	B	157	TYR	OH	C	179	LYS	HN	2.0	
	B	176	LYS	HZ2	C	49	GLU	OE1	1.7	O
6	B	49	GLU	OE1	C	176	LYS	HZ2	1.6	O
	B	128	LYS	HZ1	C	150	GLN	OE1	2.3	
	B	131	GLN	HE22	C	143	GLU	OE2	1.9	
	B	132	ASP	OD1	C	150	GLN	HE21	1.8	
	B	143	GLU	OE2	C	131	GLN	HE22	1.8	
	B	168	GLU	OE2	C	172	LYS	HZ2	1.7	O
	B	172	LYS	HZ1	C	168	GLU	OE1	1.6	O
	B	177	LYS	HZ3	C	1	SER	O	1.8	
7	B	1	SER	OG	C	175	LYS	HZ1	1.8	
	B	2	THR	OG1	C	172	LYS	HZ1	2.5	
	B	47	ASP	OD2	C	169	LYS	HZ2	1.8	O
	B	49	GLU	OE2	C	172	LYS	HZ3	1.6	O
	B	135	ARG	HE	C	153	ASP	OD2	1.8	O
	B	135	ARG	HH22	C	149	ARG	O	1.9	
	B	162	GLU	OE2	C	165	LYS	HZ3	1.6	O
	B	164	ARG	HH12	C	168	GLU	OE1	2.5	O
8	B	164	ARG	HH12	C	168	GLU	OE2	1.8	O
	B	172	LYS	HZ1	C	49	GLU	OE1	1.6	O
	B	175	LYS	HN	C	48	GLY	O	1.9	
	B	175	LYS	O	C	50	THR	HG1	2.0	

	B	177	LYS	HN	C	50	THR	OG1	2.1	
	B	178	LYS	HZ1	C	51	CYS	O	2.2	
	B	178	LYS	HZ2	C	50	THR	O	2.4	
9	B	49	GLU	OE2	C	172	LYS	HZ1	1.6	O
	B	50	THR	OG1	C	176	LYS	HZ3	1.7	
	B	132	ASP	OD1	C	150	GLN	HE21	2.1	
	B	162	GLU	OE2	C	165	LYS	HZ3	1.6	O
	B	172	LYS	HZ1	C	4	TYR	OH	1.9	
	B	172	LYS	HZ3	C	49	GLU	OE1	2.2	O
	B	172	LYS	HZ3	C	49	GLU	OE2	1.7	O
	B	175	LYS	O	C	50	THR	HG1	2.0	
	B	178	LYS	HZ3	C	43	GLN	OE1	1.8	
10	B	49	GLU	OE1	C	172	LYS	HZ1	1.6	O
	B	135	ARG	HE	C	143	GLU	O	2.5	O
	B	143	GLU	OE2	C	131	GLN	HE22	2.3	
	B	150	GLN	OE1	C	135	ARG	HE	1.9	
	B	150	GLN	OE1	C	135	ARG	HH22	2.1	
	B	162	GLU	OE1	C	161	ARG	HH22	1.7	O
	B	165	LYS	HZ3	C	162	GLU	OE2	1.6	O
	B	172	LYS	HZ3	C	49	GLU	OE1	1.7	O
	B	175	LYS	HN	C	48	GLY	O	1.9	
	B	179	LYS	HN	C	43	GLN	OE1	1.8	O
11	B	48	GLY	O	C	176	LYS	HZ3	1.6	
	B	49	GLU	OE1	C	172	LYS	HZ1	1.6	O
	B	143	GLU	OE1	C	131	GLN	HE22	2.2	
	B	150	GLN	HE22	C	132	ASP	OD1	2.2	
	B	162	GLU	OE2	C	165	LYS	HZ3	1.6	O
	B	165	LYS	HZ3	C	162	GLU	OE2	1.8	O
	B	172	LYS	HZ3	C	49	GLU	OE1	1.7	O
12	B	131	GLN	HE22	C	143	GLU	OE2	1.9	
	B	132	ASP	OD1	C	150	GLN	HE21	1.8	
	B	132	ASP	OD2	C	150	GLN	HE21	2.5	
	B	143	GLU	OE2	C	131	GLN	HE22	1.9	

	B	165	LYS	HZ3	C	162	GLU	OE2	1.6	O
	B	172	LYS	HZ3	C	49	GLU	OE1	1.7	O
13	B	131	GLN	HE22	C	141	PHE	O	1.9	
	B	138	GLY	O	C	161	ARG	HH11	2.3	
	B	138	GLY	O	C	161	ARG	HH21	1.8	
	B	150	GLN	HE21	C	132	ASP	OD1	2.3	
	B	162	GLU	OE2	C	165	LYS	HZ3	1.6	O
	B	172	LYS	HZ1	C	49	GLU	OE2	1.7	O
14	B	49	GLU	OE1	C	172	LYS	HZ1	1.6	O
	B	132	ASP	OD1	C	150	GLN	HE21	1.9	
	B	143	GLU	OE2	C	131	GLN	HE22	1.8	
	B	150	GLN	HE21	C	132	ASP	OD1	1.9	
	B	162	GLU	OE2	C	165	LYS	HZ3	1.7	O
	B	172	LYS	HZ1	C	49	GLU	OE1	1.7	O
	B	177	LYS	HN	C	1	SER	OG	1.8	
	B	177	LYS	O	C	1	SER	HG	2.1	
	B	178	LYS	HZ1	C	43	GLN	OE1	1.9	
	B	179	LYS	HZ2	C	3	GLU	OE1	1.6	O
	B	182	LYS	HN	C	3	GLU	OE2	1.7	
15	B	49	GLU	OE1	C	172	LYS	HZ1	1.6	O
	B	128	LYS	HZ2	C	150	GLN	OE1	1.9	
	B	128	LYS	HZ3	C	118	CYS	O	1.8	
	B	132	ASP	OD1	C	150	GLN	HE21	1.8	
	B	132	ASP	OD2	C	150	GLN	HE21	2.3	
	B	135	ARG	HE	C	154	ASP	OD2	2.1	O
	B	143	GLU	O	C	131	GLN	HE22	2.3	
	B	150	GLN	HE21	C	132	ASP	OD1	2.3	
	B	172	LYS	HZ3	C	168	GLU	OE1	1.7	O
	B	176	LYS	HZ2	C	50	THR	OG1	2.1	
	B	181	SER	HG	C	3	GLU	OE1	1.7	
	B	184	LYS	O	C	70	GLN	HE21	1.9	
16	B	49	GLU	OE2	C	172	LYS	HZ3	1.6	O
	B	132	ASP	OD1	C	150	GLN	HE21	2.0	

	B	143	GLU	OE2	C	131	GLN	HE22	2.3	
	B	150	GLN	HE21	C	132	ASP	OD1	1.9	
	B	43	GLN	OE1	C	179	LYS	HZ3	2.2	
	B	49	GLU	OE1	C	172	LYS	HZ3	1.6	O
	B	131	GLN	HE22	C	143	GLU	OE2	1.8	
	B	143	GLU	OE2	C	131	GLN	HE22	1.7	
	B	162	GLU	OE1	C	161	ARG	HH22	2.0	O
	B	162	GLU	OE2	C	161	ARG	HH22	2.5	O
	B	172	LYS	HZ2	C	2	THR	OG1	1.8	
	B	172	LYS	HZ3	C	49	GLU	OE2	1.6	O
	B	175	LYS	HN	C	48	GLY	O	1.7	
	B	175	LYS	HZ2	C	49	GLU	OE1	1.6	O
	B	175	LYS	O	C	50	THR	HG1	2.4	
17	B	1	SER	HG	C	178	LYS	O	1.9	
	B	47	ASP	OD2	C	169	LYS	HZ2	1.6	O
	B	49	GLU	OE1	C	172	LYS	HZ1	2.5	O
	B	49	GLU	OE1	C	175	LYS	HZ3	1.6	O
	B	49	GLU	OE2	C	172	LYS	HZ1	1.7	O
	B	131	GLN	HE22	C	143	GLU	OE2	1.8	
	B	143	GLU	OE2	C	131	GLN	HE22	1.8	
	B	143	GLU	O	C	135	ARG	HH22	1.8	
	B	168	GLU	OE1	C	164	ARG	HH12	1.8	O
	B	172	LYS	HZ3	C	49	GLU	OE2	1.6	O
18	B	49	GLU	OE1	C	172	LYS	HZ1	1.6	O
	B	131	GLN	HE22	C	143	GLU	OE2	1.8	
	B	143	GLU	OE2	C	131	GLN	HE22	1.9	
	B	150	GLN	HE21	C	132	ASP	OD1	2.5	
	B	150	GLN	HE21	C	183	THR	O	2.1	
	B	153	ASP	OD1	C	179	LYS	HZ1	1.6	O
	B	153	ASP	OD2	C	182	LYS	HZ3	1.6	O
	B	154	ASP	OD1	C	182	LYS	HZ1	2.1	O
	B	154	ASP	OD2	C	182	LYS	HZ1	1.7	O
	B	177	LYS	HZ1	C	1	SER	OG	1.7	

	B	179	LYS	HN	C	43	GLN	OE1	1.8	
	B	182	LYS	HZ1	C	41	ARG	O	1.8	
19	B	49	GLU	OE1	C	172	LYS	HZ1	1.8	O
	B	141	PHE	O	C	131	GLN	HE22	1.8	
	B	143	GLU	HN	C	131	GLN	OE1	2.1	
	B	164	ARG	HE	C	168	GLU	OE1	1.7	O
	B	168	GLU	OE1	C	167	LYS	HZ2	1.6	O
	B	172	LYS	HZ3	C	49	GLU	OE1	1.6	O
	B	175	LYS	O	C	1	SER	HG	1.7	
20	B	49	GLU	OE1	C	172	LYS	HZ2	1.7	O
	B	132	ASP	OD1	C	150	GLN	HE21	1.8	
	B	143	GLU	OE1	C	131	GLN	HE22	2.1	
	B	143	GLU	O	C	135	ARG	HH22	1.9	O
	B	175	LYS	HN	C	48	GLY	O	2.0	

[*] Cutoff distance to define a hydrogen bond is 2.5 Å.
[#] A hydrogen bond in an ion-pair interaction is indicated as “O”

Table S5. Violation analysis of PRE-derived restraints obtained from the membrane-bound KRAS-GTPγS dimer versus crystal structure of membrane-free KRAS-GTPγS dimer (PDB ID: 5VQ6).

Chain	Residue Number	Atom Name*	Chain	Residue Number	Atom Name	Distance (Å)	Average Distance (Å)	PRE Distance Restraint (Å)	Distance Violation	Result#
A	118	OG	B	44	CG1	15.5	15.0	15.4 ± 3.0		S
A	118	OG	B	44	CG2	14.3				
B	118	OG	A	44	CG1	15.7				
B	118	OG	A	44	CG2	14.5				
A	118	OG	B	45	CG1	9.1	10.2	14.4 ± 3.0	1.2	V
A	118	OG	B	45	CG2	11.1				
B	118	OG	A	45	CG1	9.3				
B	118	OG	A	45	CG2	11.2				
A	118	OG	B	46	CD1	14.2	14.3	15.7 ± 3.0		S
B	118	OG	A	46	CD1	14.4				
A	118	OG	B	142	CD1	20.3	20.3	13.3 ± 3.0	4.0	V
B	118	OG	A	142	CD1	20.3				
A	118	OG	B	160	CG1	15.9	16.6	16.0 ± 3.0		S
A	118	OG	B	160	CG2	17.4				
B	118	OG	A	160	CG1	15.9				
B	118	OG	A	160	CG2	17.4				
A	118	OG	B	127	CG2	31.8	31.8	15.2 ± 3.0	13.6	V
B	118	OG	A	127	CG2	31.8				
A	118	OG	B	142	CG2	22.0	22.0	13.8 ± 3.0	5.2	V
B	118	OG	A	142	CG2	22.1				
A	118	OG	B	144	CG2	24.1	24.1	13.7 ± 3.0	7.4	V
B	118	OG	A	144	CG2	24.2				
A	118	OG	B	148	CG2	28.3	28.3	14.4 ± 3.0	10.9	V
B	118	OG	A	148	CG2	28.3				

* In the crystal structure (PDB ID: 5VQ6), the gamma-oxygen atom (OG) of Ser118 is substituted for the gamma-sulfur atom (SG) of Cys118. Distances from Lys169 are excluded in the violation analysis because this residue is invisible in the crystallographic dimer.

"S" and "V" represent satisfaction and violation, respectively, of experimental PRE distance restraints by the crystal structure of the KRAS dimer.

Table S6. Violation analysis of PRE-derived restraints obtained from the membrane-bound KRAS-GDP dimer versus crystal structure of membrane-free KRAS-GDP dimer (PDB ID: 5W22).

Chain	Residue Number	Atom Name*	Chain	Residue Number	Atom Name	Distance (Å)	Average Distance (Å)	PRE Distance Restraint (Å)	Distance Violation	Result#
A	118	OG	B	112	CG1	22.6	22.0	15.3 ± 3.0	3.7	V
A	118	OG	B	112	CG2	21.8				
B	118	OG	A	112	CG1	22.5				
B	118	OG	A	112	CG2	21.7				
A	118	OG	B	113	CD1	29.87	29.6	14.9 ± 3.0	11.7	V
A	118	OG	B	113	CD2	29.5				
B	118	OG	A	113	CD1	29.8				
B	118	OG	A	113	CD2	29.4				
A	118	OG	B	114	CG1	25.5	25.0	17.5 ± 3.0	4.5	V
A	118	OG	B	114	CG2	24.6				
B	118	OG	A	114	CG1	25.4				
B	118	OG	A	114	CG2	24.6				
A	118	OG	B	125	CG1	34.5	35.1	16.1 ± 3.0	16.0	V
A	118	OG	B	125	CG2	35.9				
B	118	OG	A	125	CG1	34.3				
B	118	OG	A	125	CG2	35.8				
A	118	OG	B	133	CD1	34.6	34.0	14.6 ± 3.0	16.4	V
A	118	OG	B	133	CD2	33.6				
B	118	OG	A	133	CD1	34.5				
B	118	OG	A	133	CD2	33.5				
A	118	OG	B	139	CD1	28.0	28.0	15.0 ± 3.0	10.0	V
B	118	OG	A	139	CD1	27.9				
A	118	OG	B	142	CD1	19.5	19.6	14.4 ± 3.0	2.2	V
B	118	OG	A	142	CD1	19.6				
B	118	OG	A	128	N	32.1	32.0	13.1 ± 3.0	15.9	V
B	118	OG	A	128	N	32.0				
A	118	OG	B	127	CG2	30.2	30.2	13.2 ± 3.0	14.0	V
B	118	OG	A	127	CG2	30.2				
A	118	OG	B	142	CG2	21.0	21.0	14.7 ± 3.0	3.3	V
B	118	OG	A	142	CG2	21.0				

A	169	CG	B	45	CG1	31.0	31.9	15.5 ± 3.0	13.4	V
A	169	CG	B	45	CG2	32.8				
B	169	CG	A	45	CG1	31.0				
B	169	CG	A	45	CG2	32.8				
A	169	CG	B	46	CD1	26.4	26.3	15.5 ± 3.0	7.8	V
B	169	CG	A	46	CD1	26.3				
A	169	CG	B	159	CD1	21.8	22.5	16.1 ± 3.0	3.4	V
A	169	CG	B	159	CD2	23.3				
B	169	CG	A	159	CD1	21.7				
B	169	CG	A	159	CD2	23.3				
A	169	CG	B	160	CG1	25.1	25.2	14.5 ± 3.0	7.7	V
A	169	CG	B	160	CG2	25.3				
B	169	CG	A	160	CG1	25.1				
B	169	CG	A	160	CG2	25.3				
A	169	CG	B	163	CD1	25.471	25.5	15.5 ± 3.0	7.0	V
B	169	CG	A	163	CD1	25.5				
A	169	CG	B	165	N	22.4	22.4	14.8 ± 3.0	4.6	V
B	169	CG	A	165	N	22.4				
A	169	CG	B	167	N	25.8	25.8	15.3 ± 3.0	7.5	V
B	169	CG	A	167	N	25.8				
A	169	CG	B	169	N	30.0	30.0	14.8 ± 3.0	12.2	V
B	169	CG	A	169	N	29.9				
A	169	CG	B	172	N	N/A	N/A	16.1 ± 3.0	N/A	N/A
B	169	CG	A	172	N	N/A				

* In the crystal structure (PDB ID: 5W22), the gamma-oxygen atom (OG) of Ser118 is substituted for the gamma-sulfur atom (SG) of Cys118.

"S" and "V" represent satisfaction and violation, respectively, of experimental PRE distance restraints by the crystal structure of the KRAS dimer.

6. References

[1] W. K. Gillette, D. Esposito, M. Abreu Blanco, P. Alexander, L. Bindu, C. Bittner, O. Chertov, P. H. Frank, C. Grose, J. E. Jones, Z. Meng, S. Perkins, Q. Van, R. Ghirlando, M. Fivash, D. V. Nissley, F. McCormick, M. Holderfield, A. G. Stephen, *Sci Rep* **2015**, *5*, 15916.

[2] a) M. T. Mazhab-Jafari, C. B. Marshall, P. B. Stathopulos, Y. Kobashigawa, V. Stambolic, L. E. Kay, F. Inagaki, M. Ikura, *J Am Chem Soc* **2013**, *135*, 3367-3370; b) M. T. Mazhab-Jafari, C. B. Marshall, M. J. Smith, G. M. Gasmi-Seabrook, P. B. Stathopulos, F. Inagaki, L. E. Kay, B. G. Neel, M. Ikura, *Proc Natl Acad Sci U S A* **2015**, *112*, 6625-6630.

[3] F. Hagn, M. L. Nasr, G. Wagner, *Nat Protoc* **2018**, *13*, 79-98.

[4] R. Spencer-Smith, A. Koide, Y. Zhou, R. R. Eguchi, F. Sha, P. Gajwani, D. Santana, A. Gupta, M. Jacobs, E. Herrero-Garcia, J. Cobbert, H. Lavoie, M. Smith, T. Rajakulendran, E. Dowdell, M. N. Okur, I. Dementieva, F. Sicheri, M. Therrien, J. F. Hancock, M. Ikura, S. Koide, J. P. O'Bryan, *Nat Chem Biol* **2017**, *13*, 62-68.

[5] V. Tugarinov, P. M. Hwang, J. E. Ollerenshaw, L. E. Kay, *J Am Chem Soc* **2003**, *125*, 10420-10428.

[6] F. Delaglio, S. Grzesiek, G. W. Vuister, G. Zhu, J. Pfeifer, A. Bax, *J Biomol NMR* **1995**, *6*, 277-293.

[7] B. A. Johnson, *Methods Mol Biol* **2004**, *278*, 313-352.

[8] J. L. Battiste, G. Wagner, *Biochemistry* **2000**, *39*, 5355-5365.

[9] G. C. P. van Zundert, J. Rodrigues, M. Trellet, C. Schmitz, P. L. Kastritis, E. Karaca, A. S. J. Melquiond, M. van Dijk, S. J. de Vries, A. Bonvin, *J Mol Biol* **2016**, *428*, 720-725.

[10] S. Jo, J. B. Lim, J. B. Klauda, W. Im, *Biophys J* **2009**, *97*, 50-58.

[11] A. T. Brunger, *Nat Protoc* **2007**, *2*, 2728-2733.

[12] J. Iwahara, C. D. Schwieters, G. M. Clore, *J Am Chem Soc* **2004**, *126*, 5879-5896.

[13] H. Lavoie, M. Therrien, *Nat Rev Mol Cell Biol* **2015**, *16*, 281-298.

[14] a) C. Kiel, T. Selzer, Y. Shaul, G. Schreiber, C. Herrmann, *Proc Natl Acad Sci U S A* **2004**, *101*, 9223-9228; b) C. Kiel, L. Serrano, *Sci Signal* **2009**, *2*, ra38; c) C. Kiel, D. Aydin, L. Serrano, *PLoS Comput Biol* **2008**, *4*, e1000245.

[15] a) Y. Zhou, C. O. Wong, K. J. Cho, D. van der Hoeven, H. Liang, D. P. Thakur, J. Luo, M. Babic, K. E. Zinsmaier, M. X. Zhu, H. Hu, K. Venkatachalam, J. F. Hancock, *Science* **2015**, *349*, 873-876; b) Y. Zhou, P. Prakash, H. Liang, K. J. Cho, A. A. Gorfe, J. F. Hancock, *Cell* **2017**, *168*, 239-251 e216.

[16] H. Murakoshi, R. Iino, T. Kobayashi, T. Fujiwara, C. Ohshima, A. Yoshimura, A. Kusumi, *Proc Natl Acad Sci U S A* **2004**, *101*, 7317-7322.